CP3-Origins-2015-009 DNRF90, DESY 15-062,
DIAS-2015-9, HU-EP-15/16, IFT-UAM/CSIC-15-043,
LPT-Orsay/15-31, MITP/15-025, MS-TP-15-07, TCDMATH 15-04

B-meson spectroscopy in HQET at order $1/m$

ALPHA Collaboration

Fabio Bernardoni[a,b], Benoît Blossier[c], John Bulava[e], Michele Della Morte[f,g], Patrick Fritzsch[h,i], Nicolas Garron[e], Antoine Gérardin[c,d], Jochen Heitger[j], Georg von Hippel[k], Hubert Simma[a]

[a] John von Neumann Institut for Computing (NIC), DESY, Platanenallee 6, 15738 Zeuthen, Germany
[b] Medizinische Fakultät, Carl Gustav Carus, TU Dresden, Fetscherstraße 74, 01307 Dresden, Germany
[c] Laboratoire de Physique Théorique, Université Paris XI, 91405 Orsay Cedex, France
[d] Laboratoire de Physique Corpusculaire, Université Blaise Pascal, CNRS/IN2P3 63177 Aubière Cedex, France
[e] School of Computing and Mathematics, Plymouth University, PL4 8AA Plymouth, UK
[f] CP^3-Origins & Danish IAS, University of Southern Denmark, Campusvej 55, 5230 Odense M, Denmark
[g] IFIC and CSIC, Calle Catedrático José Beltran 2, 46980 Paterna, Valencia, Spain
[h] Institut für Physik, Humboldt-Universität zu Berlin, Newtonstr. 15, 12489 Berlin, Germany
[i] Instituto de Física Teórica UAM/CSIC, Universidad Autónoma de Madrid, C/ Nicolás Cabrera 13-15, Cantoblanco E-28049 Madrid, Spain
[j] Institut für Theoretische Physik, Universität Münster, Wilhelm-Klemm-Str. 9, 48149 Münster, Germany
[k] Institut für Kernphysik, University of Mainz, Becherweg 45, 55099 Mainz, Germany

Abstract

We present a study of the B spectrum performed in the framework of Heavy Quark Effective Theory expanded to next-to-leading order in $1/m_\mathrm{b}$ and non-perturbative in the strong coupling. Our analyses have been performed on $N_\mathrm{f} = 2$ lattice gauge field ensembles corresponding to three different lattice spacings and a wide range of pion masses. We obtain the $\mathrm{B_s}$-meson mass and hyperfine splittings of the B- and $\mathrm{B_s}$-mesons that are in good agreement with the experimental values and examine the mass difference $m_{\mathrm{B_s}} - m_\mathrm{B}$ as a further cross-check of our previous estimate of the b-quark mass. We also report on the mass splitting between the first excited state and the ground state in the B and $\mathrm{B_s}$ systems.

Keywords: Lattice QCD, Heavy Quark Effective Theory, Bottom mesons, Spectroscopy
PACS: 12.38.Gc, 12.39.Hg, 14.40.Nd

1 Introduction

Lattice studies of the hadron spectrum provide valuable indications on the reliability of effective field theories. A phenomenologically relevant example is given by effective field theories for heavy quarks, such as Heavy Quark Effective Theory (HQET) or Non-Relativistic QCD (NRQCD).

In this respect, hyperfine splittings are of great theoretical interest, since they vanish in the static ($1/m_{\rm h} \to \infty$) limit, and thus serve to probe subleading terms in the heavy quark expansion. In the context of lattice NRQCD, for example, it was found that in order to obtain a determination of the hyperfine splittings of bottomonium that is consistent with experiments, the perturbative improvement of the NRQCD action to at least one-loop order is required [1–3], for values of the lattice spacing of about 0.1 fm. The Υ spectrum, on the other hand, is well reproduced within NRQCD, and has been used in the literature as a quantity to set the lattice spacing [4,5]. Hyperfine splittings have also been studied within the HISQ approach to heavy quarks [6].

In contrast to other studies, our results are based on non-perturbatively renormalized HQET including the next-to-leading order in the inverse heavy quark mass. Regarding specifically the B spectrum, it is well known that the masses of the pseudoscalar B_q and vector B_q^* differ as a result of spin effects [7]. This mass difference is produced in HQET by a $\mathrm{O}(1/m_{\rm h})$ chromomagnetic term in the Lagrangian that breaks the heavy quark spin symmetry of the static theory [8,9].

Another quantity of interest is the SU(3) isospin breaking quantity $m_{\mathrm{B_s}} - m_{\mathrm{B}}$. Most of the dependence on the heavy quark mass cancels in the difference and the statistical correlations between the strange and light-quark measurements should lead to a much improved precision in the determination of the difference compared to what would be possible for the individual masses. In [10], the mass of the B-meson has been used to determine the b-quark mass. Since the mass of the $\mathrm{B_s}$-meson could have equally well been used, it is instructive to study how the strange-light mass difference propagates to the b-quark mass measurement.

Relatively little is known experimentally on the radial excitations of B-mesons, usually denoted by B'. CDF has claimed the observation of a resonant state B(5970) that may be interpreted as a B' state [11]. Lattice predictions for the radial excitation energies of the B system have been made in the framework of NRQCD [12,13] and HQET [14–22], but, with the exception of the most recent studies, control of the continuum extrapolation has been limited, if possible at all. An additional difficulty that always needs to be addressed is in disentangling single particle excitations from multi-particle states. We use the notation $\mathrm{B^r}$ (or $\mathrm{B}_q^{\rm r}$ with $q = \mathrm{u/d}$ or s) for the excited states that we observe. They might be identified with radial excitations B', but without a dedicated study including also multi-hadron operators, we are unable to conclusively determine the nature of these excited states.

In this paper, we report on our estimate of the hyperfine splittings $\Delta_q^{\rm HF} m$ in the B and $\mathrm{B_s}$ systems, and on the mass differences $m_{\mathrm{B^r}} - m_{\mathrm{B}}$, $m_{\mathrm{B_s^r}} - m_{\mathrm{B_s}}$ and $m_{\mathrm{B_s}} - m_{\mathrm{B}}$ from $N_{\rm f} = 2$ lattice simulations.

	$\beta = 5.5$		$\beta = 5.3$		$\beta = 5.2$	
	HYP1	HYP2	HYP1	HYP2	HYP1	HYP2
$am_{\rm bare}^{\rm stat}$	0.969(12)	1.000(12)	1.317(15)	1.350(15)	1.520(17)	1.553(17)
$am_{\rm bare}$	0.594(14)	0.606(14)	0.993(17)	1.014(17)	1.214(18)	1.239(18)
$\omega_{\rm kin}/a$	0.520(11)	0.525(10)	0.415(8)	0.418(8)	0.377(7)	0.380(7)
$\omega_{\rm spin}/a$	0.949(37)	1.090(42)	0.73(28)	0.883(33)	0.655(24)	0.812(30)

Table 1: Values of HQET parameters at the physical point $\boldsymbol{\omega}(z = z_{\rm b})$. As determined in [10], we have used $z_{\rm b}^{\rm stat} = 13.24$ to interpolate the parameters of HQET at static order, and $z_{\rm b} = 13.25$ for the parameters of HQET expanded to NLO. The bare coupling g_0 is given by $\beta = 6/g_0^2$.

2 Theoretical setup

2.1 HQET on the lattice

Heavy Quark Effective Theory (HQET) can be formulated with a lattice regulator. The resulting lattice field theory can be non-perturbatively matched to QCD in the continuum limit. This provides a rigorous and systematically improvable approach to the study of the B-meson system. The HQET action at $\mathrm{O}(1/m_{\rm h})$ reads

$$S_{\rm HQET} = a^4 \sum_x \left\{ \mathscr{L}_{\rm stat}(x) - \omega_{\rm kin} \mathcal{O}_{\rm kin}(x) - \omega_{\rm spin} \mathcal{O}_{\rm spin}(x) \right\}, \tag{2.1}$$

$$\mathscr{L}_{\rm stat}(x) = \overline{\psi}_{\rm h}(x)\, D_0\, \psi_{\rm h}(x)\,, \tag{2.2}$$

$$\mathcal{O}_{\rm kin}(x) = \overline{\psi}_{\rm h}(x)\, \mathbf{D}^2\, \psi_{\rm h}(x)\,, \tag{2.3}$$

$$\mathcal{O}_{\rm spin}(x) = \overline{\psi}_{\rm h}(x)\, \boldsymbol{\sigma} \cdot \mathbf{B}\, \psi_{\rm h}(x)\,, \tag{2.4}$$

where the subscript h denotes a heavy (static) quark field satisfying $\frac{1+\gamma_0}{2}\psi_{\rm h} = \psi_{\rm h}$, and the operators are normalized such that the classical (tree level) values of the coefficients are $\omega_{\rm kin} = \omega_{\rm spin} = 1/(2m_{\rm h})$. The energy levels computed in this theory are relative to a bare mass $m_{\rm bare}$, which at tree level is simply $m_{\rm h}$, but has to absorb a power-divergent shift at the quantum level, implying that it will take a different value depending on whether the $\mathrm{O}(1/m_{\rm h})$ terms are included or not. The renormalizability of the static theory can be preserved at NLO by considering a strict expansion of correlation functions in $1/m_{\rm h}$,

$$\langle O \rangle = \langle O \rangle_{\rm stat} + \omega_{\rm kin}\, a^4 \sum_x \langle O\, \mathcal{O}_{\rm kin}(x) \rangle_{\rm stat} + \omega_{\rm spin}\, a^4 \sum_x \langle O\, \mathcal{O}_{\rm spin}(x) \rangle_{\rm stat}\,, \tag{2.5}$$

where the suffix "stat" denotes an expectation value measured in the static theory.

The values of the parameters $m_{\rm bare}^{\rm stat}$ and $\{m_{\rm bare}, \omega_{\rm kin}, \omega_{\rm spin}\}$ required to match to QCD have been determined in [10,23] using the Schrödinger Functional scheme. In order to keep this paper self-contained, we summarize in Table 1 their values for the three lattice spacings $a(\beta)$ and two static discretizations (HYP1, HYP2 [24]) that we use. The parameters are given at $z_{\rm b} = L_1 M_{\rm b}$ where $M_{\rm b}$ is the Renormalization Group Invariant (RGI) b-quark mass and L_1 is the linear extent of the lattice used for the matching.

2.2 The variational method

For spectroscopic applications, having good control over contributions from excited states is crucial to reduce the systematic error on the determination of the ground state. For this

purpose it is necessary to use a variational method [25–29], which starts from matrices of correlation functions,

$$\begin{aligned} C_{ij}^{\rm stat}(t) &= \sum_{x,\mathbf{y}} \left\langle O_i(x_0+t,\mathbf{y})\, O_j^*(x) \right\rangle_{\rm stat} , \\ C_{ij}^{\rm kin/spin}(t) &= \sum_{x,\mathbf{y},z} \left\langle O_i(x_0+t,\mathbf{y})\, O_j^*(x)\, \mathcal{O}_{\rm kin/spin}(z) \right\rangle_{\rm stat} , \end{aligned} \tag{2.6}$$

containing all pairwise correlators of some set of interpolating fields $O_i\,,\ i = 1,\ldots,N$, and proceeds to solve the generalized eigenvalue problem (GEVP)

$$C^{\rm stat}(t)\, v_n^{\rm stat}(t,t_0) = \lambda_n^{\rm stat}(t,t_0)\, C^{\rm stat}(t_0)\, v_n^{\rm stat}(t,t_0)\,, \quad n = 1,\ldots,N\,, \quad t > t_0\,. \tag{2.7}$$

From the generalized eigenvalues $\lambda_n^{\rm stat}(t,t_0)$ and the corresponding eigenvectors $v_n^{\rm stat}(t,t_0)$, the effective energy levels can be computed as [29, 30]

$$\begin{aligned} E_n^{\rm eff,stat}(t,t_0) &= -\frac{1}{a}\left[\log\lambda_n^{\rm stat}(t+a,t_0) - \log\lambda_n^{\rm stat}(t,t_0)\right], \\ E_n^{\rm eff,x}(t,t_0) &= \frac{\lambda_n^{\rm x}(t,t_0)}{\lambda_n^{\rm stat}(t,t_0)} - \frac{\lambda_n^{\rm x}(t+a,t_0)}{\lambda_n^{\rm stat}(t+a,t_0)}\,, \end{aligned} \tag{2.8}$$

where $\mathrm{x} \in \{\mathrm{kin}, \mathrm{spin}\}$ and

$$\frac{\lambda_n^{\rm x}(t,t_0)}{\lambda_n^{\rm stat}(t,t_0)} = \left(v_n^{\rm stat}(t,t_0)\,,\, [[\lambda_n^{\rm stat}(t,t_0)]^{-1}\, C^{\rm x}(t) - C^{\rm x}(t_0)] v_n^{\rm stat}(t,t_0)\right)\,. \tag{2.9}$$

The corresponding asymptotic behaviour is known to be

$$E_n^{\rm eff,stat}(t,t_0) = E_n^{\rm stat} + \beta_n^{\rm stat}\, \mathrm{e}^{-\Delta E_{N+1,n}^{\rm stat}\, t} + \ldots\,, \tag{2.10}$$

$$E_n^{\rm eff,x}(t,t_0) = E_n^{\rm x} + [\,\beta_n^{\rm x} - \beta_n^{\rm stat}\, t\, \Delta E_{N+1,n}^{\rm x}\,]\mathrm{e}^{-\Delta E_{N+1,n}^{\rm stat}\, t} + \ldots\,, \tag{2.11}$$

where the energy gap is defined as $\Delta E_{m,n} = E_m - E_n$.

In our study, the operator basis used is given by heavy-light bilinears with varying levels of Gaussian smearing [31] applied to the light quark field,

$$O_k(x) = \overline{\psi}_{\rm h}(x)\,\gamma_0\gamma_5\,\psi_q^{(k)}(x)\,, \qquad \psi_q^{(k)}(x) = \left(1+\kappa_{\rm G}\, a^2\,\Delta\right)^{R_k}\psi_q(x)\,, \tag{2.12}$$

where $q = \mathrm{u/d}$ or s. The covariant Laplacian Δ is built from gauge links that have been triply APE smeared [32, 33] in the spatial directions, and the smearing parameters $\kappa_{\rm G}$ and R_k are chosen so as to approximately cover the same sequence of physical radii at each value of the lattice spacing, as discussed in [10]. We solve the GEVP for the matrix of correlators in the static limit for $N = 3$.

An illustration of two typical plateaux of the energies $E_1^{\rm spin}$ and $E_2^{\rm stat}$ is shown in Fig. 1. The plateau regions used for weighted averaging have been chosen by applying the procedure already discussed in [34, 35] in order to ensure that the systematic errors due to excited-state contributions are less than a given fraction (typically 1/3) of the statistical errors on the GEVP results. As a consistency check, we have also employed a global fit of the form of eqs. (2.10) and (2.11) to our data. The values of E_n obtained from the fit are compatible with the plateau values, and generally exhibit smaller statistical errors. We therefore consider our errors to be estimated conservatively.

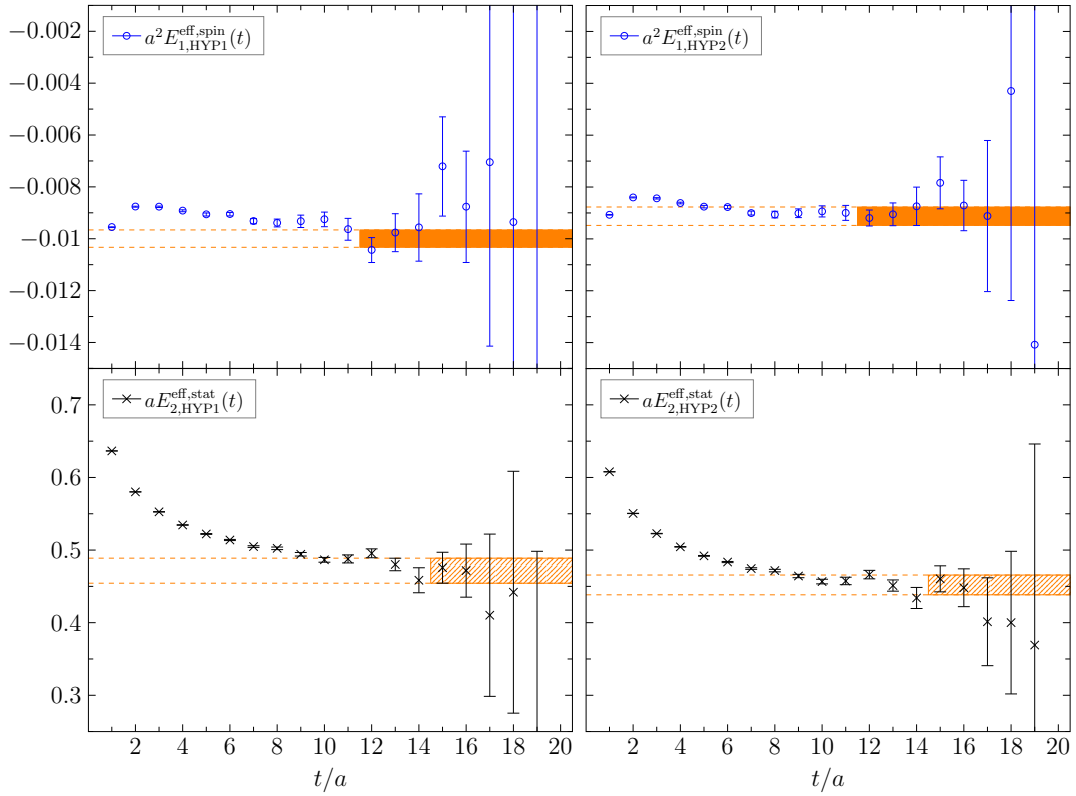

Figure 1: Illustration of typical plateaux for the $\mathrm{O}(1/m_\mathrm{b})$ chromomagnetic energy $a^2 E_1^{\mathrm{spin}}$ (*top*) and the first excited state static energy aE_2^{stat} (*bottom*), computed on the CLS ensemble N6 ($a = 0.048\,\mathrm{fm}$, $m_\pi = 340\,\mathrm{MeV}$).

2.3 Computing masses

We start by recalling the definition of the B_q-meson mass as it has been used to non-perturbatively fix the HQET parameters for the static quark discretizations HYP1 and HYP2 in [10]. On the lattice one combines the HQET parameters (see Table 1, or [36] for a more detailed discussion) with the large volume computations of ground state energies,

$$m^{\mathrm{stat}}_{\mathrm{B}_q}(m_\pi, a) = m^{\mathrm{stat}}_{\mathrm{bare}} + E_1^{\mathrm{stat}}\big|_{m_q}\,, \tag{2.13a}$$

$$m_{\mathrm{B}_q}(m_\pi, a) = m_{\mathrm{bare}} + E_1^{\mathrm{stat}}\big|_{m_q} + \omega_{\mathrm{kin}} E_1^{\mathrm{kin}}\big|_{m_q} + \omega_{\mathrm{spin}} E_1^{\mathrm{spin}}\big|_{m_q}\,. \tag{2.13b}$$

We use the subscript m_q to indicate that the corresponding energy results from the GEVP analysis of correlation functions in the heavy-light ($q = \mathrm{d}$) or heavy-strange ($q = \mathrm{s}$) sector along the lines presented in Section 2.2. The PDG value $m_\mathrm{B} = 5.2795\,\mathrm{GeV}$ in [7] has already been used as input to determine m_b [10] and thus the HQET parameters ω_i. However, re-computing m_B at fixed values of the HQET parameters serves as a non-trivial cross-check of our calculation. Additionally, we will compute $m_{\mathrm{B_s}}$ in the very same way. All remaining observables presented in the present paper are mass splittings which can be computed with the data resulting from our GEVP analysis. We now give their explicit definition before discussing any combined chiral and continuum extrapolation in Section 2.4.

e-id	β	$\kappa_{\mathrm{d}} = \kappa_{\mathrm{sea}}$	κ_{s}	τ	τ_{cfg}	τ_{exp}	heavy-light		heavy-strange	
							HYP1	HYP2	HYP1	HYP2
A4	5.2	0.135900	0.1352850	2	8	106	1012 [1,1]		1000 [1,1]	
A5c		0.135940	0.1352570	2	4	39	501 [1,1]		500 [1,1]	
A5d							500 [1,1]		–	–
B6		0.135970	0.1352390	2	2	39	636 [1,1]		636 [1,1]	
E5	5.3	0.136250	0.1357770	4	16	151	1000 [1,1]		1000 [1,1]	
F6		0.136350	0.1357410	2	8	151	500 [1,1]		600 [1,1]	
F7		0.136380	0.1357300	2	8	151	602 [100,1]		200 [1,2]	
G8		0.136417	0.1357050	2	2	56	410 [1,1]		–	–
N5	5.5	0.136600	0.1362620	0.5	8	488	477 [300,1]		–	–
N6		0.136670	0.1362500	2	4	108	950 [2,2]		707 [100,2]	
O7		0.136710	0.1362430	2	4	108	980 [1,1]		–	490 [1,2]

Table 2: Measurement details for observables in the light- and strange-quark sector. For each ensemble we list the light- and strange-quark hopping parameter, the trajectory length τ, the distance of saved configurations τ_{cfg} and the exponential autocorrelation time τ_{exp} in MDU. For each individual static quark discretization we then specify N_{ms} [m,d], i.e., the total number of measurements starting from the m^{th} saved configuration using every d^{th}. Note that for A5 we have two independent Monte-Carlo chains.

The hyperfine splitting of the B_q-meson system, $m_{\mathrm{B}_q^*} - m_{\mathrm{B}_q}$, is given by

$$\Delta_q^{\mathrm{HF}} m\,(m_\pi, a) = -\frac{4}{3}\omega_{\mathrm{spin}} E_1^{\mathrm{spin}}\big|_{m_q}\,, \qquad q = \mathrm{s}, \mathrm{d}\,, \tag{2.14}$$

and depends on the HQET parameter ω_{spin} and the large-volume measurement of E_1^{spin}. The strange-light mass difference $m_{\mathrm{B_s}} - m_{\mathrm{B_d}}$, at the static and $\mathrm{O}(1/m_{\mathrm{b}})$ level, reads,

$$\Delta_{\mathrm{s-d}}^{\mathrm{stat}} m\,(m_\pi, a) = \Delta_{\mathrm{s-d}} E_1^{\mathrm{stat}}\,, \tag{2.15a}$$

$$\Delta_{\mathrm{s-d}} m\,(m_\pi, a) = \Delta_{\mathrm{s-d}} E_1^{\mathrm{stat}} + \omega_{\mathrm{kin}}\Delta_{\mathrm{s-d}} E_1^{\mathrm{kin}} + \omega_{\mathrm{spin}}\Delta_{\mathrm{s-d}} E_1^{\mathrm{spin}}\,, \tag{2.15b}$$

respectively, where we have defined the shorthand $\Delta_{\mathrm{s-d}} Q = Q|_{m_q = m_{\mathrm{s}}} - Q|_{m_q = m_{\mathrm{d}}}$. Finally, the mass gaps for excited states, $m_{\mathrm{B}_q^{\mathrm{r}}} - m_{\mathrm{B}_q}$, can be computed from $\Delta E_{m,n} = E_m - E_n$ via

$$\Delta_{\mathrm{r},q}^{\mathrm{stat}} m\,(m_\pi, a) = \Delta E_{2,1}^{\mathrm{stat}}\big|_{m_q}\,, \tag{2.16a}$$

$$\Delta_{\mathrm{r},q} m\,(m_\pi, a) = \Delta E_{2,1}^{\mathrm{stat}}\big|_{m_q} + \omega_{\mathrm{kin}}\Delta E_{2,1}^{\mathrm{kin}}\big|_{m_q} + \omega_{\mathrm{spin}}\Delta E_{2,1}^{\mathrm{spin}}\big|_{m_q}\,, \tag{2.16b}$$

to static and $\mathrm{O}(1/m_{\mathrm{b}})$ accuracy, respectively. As any observable computed on the lattice, these quantities depend on the input parameters used in the simulation. The strange and bottom quark mass have been fixed to their physical value along the lines reported in [10,36,37], such that only the dependences on the light quark mass—here parameterized by m_π—and lattice spacing a remain.

We have extracted the energies on a subset of gauge ensembles from the Coordinated Lattice Simulations (CLS) effort for $N_{\mathrm{f}} = 2$. The parameters of the simulations and the statistics entering our analysis are collected in Table 1 of [10]. Remaining details

of the measurements have been summarized in Table 2.[1] The light quark is treated in a unitary setup with m_π in the range [190 MeV, 440 MeV], and the bare strange quark mass has been tuned on each CLS ensemble to its physical value by using the kaon decay constant f_K to set the scale [37] and $m_\mathrm{K} = 494.2\,\mathrm{MeV}$. The lattice spacings are $a/\mathrm{fm} \in \{0.048, 0.065, 0.075\}$ for $\beta \in \{5.5, 5.3, 5.2\}$, corresponding to the CLS ensemble ids N–O, E–G and A–B, respectively. All lattices have $m_\pi L \geq 4$, such that finite-volume effects are sufficiently exponentially suppressed at the level of accuracy we are working at.

Our data analysis takes into account correlations between different observables as well as intrinsic autocorrelations of the Hybrid Monte Carlo (HMC) algorithm resulting from slow modes in the simulation. As these contributions rapidly grow towards the continuum limit, it is mandatory to estimate and include a-priori unknown long-tail contributions from the autocorrelation function of each individual observable. Further details of our analysis method can be found in Appendix A.

2.4 Extrapolation to the physical point

To extrapolate our data to the continuum limit and to the physical point, we take expressions from heavy meson chiral perturbation theory (HMχPT) if available, and a linear ansatz otherwise.

In the chiral regime, the mass of the B-meson can be extrapolated to the physical point using a functional form motivated by HMχPT [38]. Defining a subtracted mass by removing the leading non-analytic (in the quark mass) term, viz.

$$m^{\mathrm{sub}}_{\mathrm{B}_q,\delta}(y,a) = m_{\mathrm{B}_q}(m_\pi,a) + c_q \frac{3\widehat{g}^2}{16\pi}\left(\frac{m_\pi^3}{f_\pi^2} - \frac{(m_\pi^{\mathrm{exp}})^3}{(f_\pi^{\mathrm{exp}})^2}\right)\,, \tag{2.17}$$

with $c_q = 1$ in HMχPT at NLO for $q = \mathrm{d}$ but zero otherwise, the parameterization reads

$$m^{\mathrm{sub}}_{\mathrm{B}_q,\delta}(y,a) = B_q + C_q\,(y - y^{\mathrm{exp}}) + D_{q,\delta}a^2\,. \tag{2.18}$$

In (2.17) the $B^*B\pi$-coupling $\widehat{g} = 0.492(29)$ is taken from [39] and $y = m_\pi^2/(8\pi^2 f_\pi^2)$ (with the convention $f_\pi^{\mathrm{exp}} = 130.4\,\mathrm{MeV}$ and $m_\pi^{\mathrm{exp}} = 134.98\,\mathrm{MeV}$). We use the same set of measurements for f_π and m_π on each CLS ensemble as reported in foregoing analyses [10, 36]. We add the subscript δ to distinguish the two available static discretizations which are combined in the extrapolation to obtain the parameter $B_q \equiv m_{\mathrm{B}_q}$ at the physical point $(y,a) = (y^{\mathrm{exp}},0)$. For the B_q-meson mass an extrapolation quadratically in the lattice spacing is justified as we have full $\mathrm{O}(a)$ improvement at work in (2.13) at the static order and $\mathrm{O}(a)$ terms are then suppressed by a factor $1/m_\mathrm{b}$ once NLO terms in HQET are taken into account. For the case of m_B that has been explicitly checked in [10] and it is therefore conceivably valid also here for $m_{\mathrm{B_s}}$.

In Fig. 2 we show the continuum and chiral extrapolations of $m_{\mathrm{B_s}}$ and $m_{\mathrm{B_s}} - m_\mathrm{B}$ at next-to-leading order in $1/m_\mathrm{b}$. In this and the following Figures, filled symbols and dashed curves represent our HYP1 data set, while open symbols and dash-dotted curves represent our HYP2 data set. For both, equal colours and symbols refer to the same lattice spacing as indicated by equal values of the bare gauge coupling, given by $\beta = 6/g_0^2$ in the legend,

[1] For the B6-ensemble a preliminary value of κ_s has been used, which produces a bare subtracted quark mass which differs by about 1 MeV from the final one.

c.f. Tables 1 and 2. The solid black line is the continuum limit given by the part of the fit function which is independent of the lattice spacing a. Accordingly, the difference between the solid and non-solid lines represents the cutoff effect as fitted through a given ansatz.

For the hyperfine splitting, we can perform the chiral and continuum extrapolation using

$$\Delta^{\mathrm{HF}}_{q,\delta} m\,(y,a) = [m_{\mathrm{B}^*_q} - m_{\mathrm{B}_q}]\left[1 - \bar{c}_q \tfrac{3}{2}\widehat{g}^2\,(y\ln y - y^{\mathrm{exp}}\ln y^{\mathrm{exp}}) + \bar{C}_q\,(y - y^{\mathrm{exp}})\right] + \bar{D}_{q,\delta}\,a + \bar{\bar{D}}_{q,\delta}\,a^2\,, \tag{2.19}$$

with the continuum part coinciding, in the case $q = \mathrm{d}$, with the expression derived in [40]. Hence, we can probe two ansätze for the chiral extrapolation by setting $\bar{c}_{\mathrm{d}} = 0, 1$. Since in principle the $\mathrm{O}(a)$ improvement of the hyperfine splitting is not implemented, we have included linear cutoff effects, but also study the scaling behaviour with an $\mathrm{O}(a^2)$ ansatz by setting either $\bar{D}_{q,\delta}$ or $\bar{\bar{D}}_{q,\delta}$ to zero in the equation above. In general, our data is not sensitive enough to clearly separate $\mathrm{O}(a)$ scaling from $\mathrm{O}(a^2)$ such that individual fits lead to similar results. As additional safety measure we account for a systematic error by increasing the uncertainty of the favoured $\mathrm{O}(a)$ extrapolation in order to cover the mean value obtained from the corresponding $\mathrm{O}(a^2)$ extrapolation. As will be seen in the following, this only occurs in the case of $m_{\mathrm{B}^*_{\mathrm{s}}} - m_{\mathrm{B}_{\mathrm{s}}}$.

Since, to our knowledge, no systematic HMχPT formulae exist in the literature for the mass splittings $m_{\mathrm{B}^{\mathrm{r}}_q} - m_{\mathrm{B}_q}$, we again employ a simple linear ansatz in m_π^2:

$$\Delta^{\mathrm{stat}}_{\mathrm{r},q} m\,(y,a) = [m_{\mathrm{B}^{\mathrm{r}}_q} - m_{\mathrm{B}_q}]^{\mathrm{stat}} + C^{\mathrm{stat}}_q (y - y^{\mathrm{exp}}) + E^{\mathrm{stat}}_{q,\delta} a^2\,, \tag{2.20}$$

$$\Delta_{\mathrm{r},q} m\,(y,a) = [m_{\mathrm{B}^{\mathrm{r}}_q} - m_{\mathrm{B}_q}] + C'_q (y - y^{\mathrm{exp}}) + E'_{q,\delta} a + E''_{q,\delta} a^2\,. \tag{2.21}$$

For the mass splitting $\Delta_{\mathrm{r},q} m$ at next-to-leading order in HQET, one can in fact define

$$\Delta^{1/\mathrm{m}}_{\mathrm{r},q} m\,(y,a) \equiv \Delta_{\mathrm{r},q} m\,(y,a) - \Delta^{\mathrm{stat}}_{\mathrm{r},q} m\,(y,a) \tag{2.22}$$

and take the continuum limit of the leading (static) and next-to-leading order piece (1/m) separately. While for the former eq. (2.20) can be employed, the $1/m_{\mathrm{b}}$-correction term has to be extrapolated using ansatz (2.21) with $E''_{q,\delta} = 0$. Both pieces can again be combined after the physical point is reached, leading to an improved signal that is dominated by the static extrapolation. No matter what way is pursued, all extrapolations lead to results that are well compatible within errors.

We perform the full analysis using two static discretizations (HYP1,HYP2) while only one may already suffice. The reason is that the universality of the continuum limit, a property that can be rigorously guaranteed for renormalizable theories, implies that both static discretizations have to lead to equal results in the continuum. At finite lattice spacing the two discretizations have inherently different lattice artifacts, best seen among our observables in Fig. 3. To this end one can either take the two independently in order to show that universality holds or—as we usually do—combine both in one fit in order to stabilise the χ^2-minimization. It furthermore serves as a non-trivial check that the whole procedure has been applied correctly and consistently.

3 Results

Using the HQET parameters of Table 1 at $z_{\mathrm{b}} = 13.25$, we obtain for the B-meson mass $m_{\mathrm{B}} = 5.285(62)\,\mathrm{GeV}$ by employing eqs. (2.17) and (2.18) with $c_q = 1$ as extrapolation

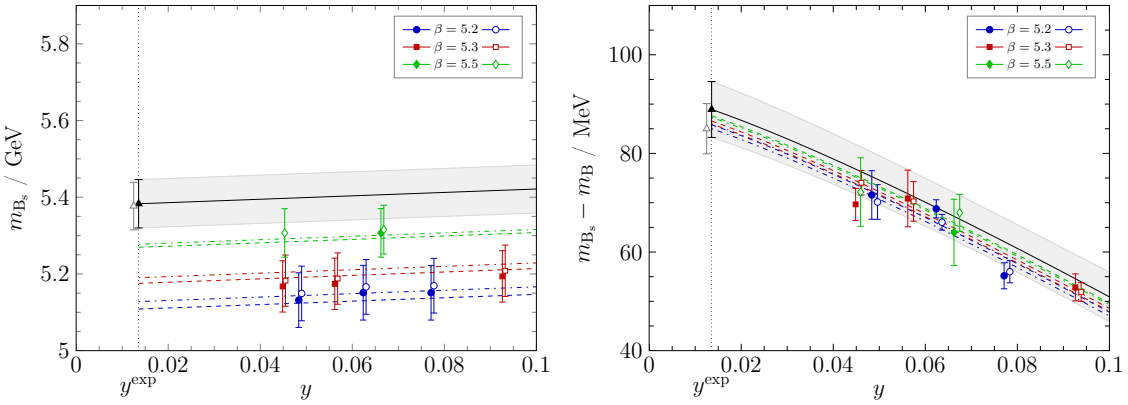

Figure 2: Chiral and continuum extrapolation of m_{B_s} (*left*) and $m_{B_s} - m_B$ (*right*) according to (2.18). The open triangle represents the corresponding result for extrapolating the static order data. Here and in the following Figures, filled symbols and dashed curves represent our HYP1 data set, while open symbols and dash-dotted curves represent our HYP2 data set. The solid black line is the continuum limit for the given fit ansatz.

ansatz. Note, however, that the experimental value $m_B = 5.2795$ GeV has been used as input in [10] to fix the b-quark mass. Therefore m_B is not a prediction of the theory in our setup, and the number above should be regarded as a consistency check of the approach.

3.1 Ground states

As first quantities beyond m_B, we compute the B_s-meson mass and the mass difference $m_{B_s} - m_B$. Their continuum and chiral extrapolations at next-to-leading order in $1/m_b$ are shown in Fig. 2 and compared to the extrapolated value of the static data at the physical point. The raw data for the mass difference $m_{B_s} - m_B$ and the hyperfine splittings is collected in Tables 3 and 4.

From the extrapolation of the form of eqs. (2.17) and (2.18) with $c_q = 0$, we obtain the result:

$$m_{B_s} = 5383(63)\,\text{MeV}\,, \qquad m_{B_s} - m_{B_s}^{\text{stat}} = 58(12)\,\text{MeV}\,, \tag{3.1}$$

where the error includes statistic and systematic uncertainties (scale setting, HQET parameters), combined in quadrature as explained in Appendix A. Although our result for m_{B_s} comes with a much larger error compared to the PDG value, $m_{B_s^0} = 5366.77 \pm 0.24\,\text{MeV}$, the difference between the mean values is only one fourth of our error.

In the combination $m_{B_s} - m_B$, the error is reduced due to correlations among the heavy-light and heavy-strange measurements, although the latter have been performed on a subset of the available ensembles only, as it can be inferred from Table 2.

Our results for the B_s-B mass splitting at $O(1/m)$ and in the static approximation are

$$m_{B_s} - m_B = 88.9(5.7)(2.3)_\chi\,\text{MeV}\,, \tag{3.2a}$$
$$[m_{B_s} - m_B]^{\text{stat}} = 85.0(5.1)(2.2)_\chi\,\text{MeV}\,, \tag{3.2b}$$

both in good agreement with the PDG value of [7] $m_{B_s} - m_B = 87.35(23)\,\text{MeV}$. Here, the quoted mean and statistical error results from an HMχPT extrapolation ansatz that

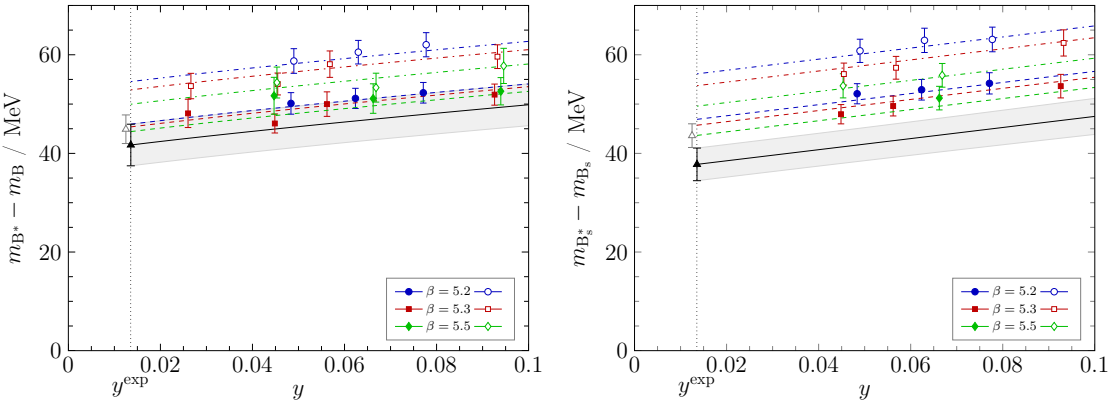

Figure 3: Chiral and continuum extrapolation of the hyperfine spin splitting of the B-meson (*left*) and of the B_s-meson (*right*). For $m_{B^*} - m_B$ we show the extrapolation from ansatz (2.19) with $\bar{c}_d = 1$ and leading a-effects, while for $m_{B_s^*} - m_{B_s}$ we have to set $\bar{c}_s = 0$. In both panels the open triangle at the physical point reflects the corresponding fit result using an a^2-scaling ansatz. Details are given in Table 3.

		$\Delta_{s-d} m$ [MeV]		$\Delta^{stat}_{s-d} m$ [MeV]	
e-id	y	HYP1	HYP2	HYP1	HYP2
A4	0.0771(14)	55.2(2.6)	56.0(2.3)	51.9(2.1)	53.1(1.8)
A5	0.0624(13)	68.8(1.8)	66.0(1.6)	62.6(1.8)	63.4(1.7)
B6	0.0484(9)	71.6(4.9)	70.2(3.5)	66.5(3.9)	67.3(3.1)
E5	0.0926(15)	52.8(2.7)	51.9(1.9)	48.8(2.0)	49.2(1.7)
F6	0.0562(9)	70.9(5.7)	70.3(4.0)	66.5(5.2)	64.7(3.9)
F7	0.0449(8)	69.7(3.2)	74.0(2.5)	67.1(3.0)	69.4(2.4)
N6	0.0662(10)	64.0(6.7)	68.0(3.7)	62.8(4.8)	63.3(3.2)
O7	0.0447(7)	–	72.2(6.9)	–	70.2(5.3)
LO-a^2	$y^{exp}, a = 0$	91.2(5.8)		87.2(5.2)	
NLO-a^2	$y^{exp}, a = 0$	88.9(5.7)		85.0(5.1)	

Table 3: Mass splitting between B_s- and B_d-meson at static and next-to-leading order HQET.

is obtained by appropriately combining eq. (2.18) for the light and strange quark sector. As systematic error due to the chiral extrapolation ansatz we quote its difference to the standard m_π^2-extrapolation.

For the hyperfine spin splittings, we obtain

$$m_{B^*} - m_B = 41.7(4.2)(3.2)_a(0.3)_\chi \,\text{MeV} \,, \tag{3.3a}$$

$$m_{B_s^*} - m_{B_s} = 37.8(3.3)(5.8)_a \,\text{MeV} \,, \tag{3.3b}$$

where we quote the mean value obtained with $\bar{c}_d = 1$ for the B-meson case and add the difference w.r.t. the result obtained from the ansatz with $\bar{c}_d = 0$ as a systematic error estimate for the chiral extrapolation. As mentioned earlier, we also account here for a systematic error between linear and quadratic continuum extrapolations. The $O(a)$ extrapolations are shown for both the B and the B_s system in Fig. 3. The filled/empty symbols at the physical point are the results using either an $O(a)$, or an $O(a^2)$ term in the continuum extrapolation.

		$\Delta_{\rm d}^{\rm HF} m$ [MeV]		$\Delta_{\rm s}^{\rm HF} m$ [MeV]	
e-id	y	HYP1	HYP2	HYP1	HYP2
A4	0.0771(14)	52.3(2.1)	62.0(2.4)	54.2(2.2)	63.1(2.5)
A5	0.0624(13)	51.1(2.0)	60.5(2.4)	52.9(2.1)	62.9(2.5)
B6	0.0484(9)	50.1(2.2)	58.7(2.5)	52.1(2.0)	60.8(2.4)
E5	0.0926(15)	51.9(2.1)	59.6(2.4)	53.6(2.4)	62.4(2.7)
F6	0.0562(9)	50.0(2.5)	58.1(2.7)	49.6(2.0)	57.4(2.3)
F7	0.0449(8)	46.1(1.9)	54.1(2.2)	47.9(2.0)	56.1(2.2)
G8	0.0260(5)	48.1(2.9)	53.7(2.6)	–	–
N5	0.0940(19)	52.6(2.8)	57.7(3.6)	–	–
N6	0.0662(10)	51.1(3.0)	53.3(2.9)	51.2(2.4)	55.8(2.4)
O7	0.0447(7)	51.7(3.7)	54.4(3.1)	–	53.7(2.4)
LO-a^2	$y^{\rm exp}, a = 0$	45.2(2.9)		43.6(2.4)	
LO-a^1	$y^{\rm exp}, a = 0$	42.0(4.2)		37.8(3.3)	
NLO-a^2	$y^{\rm exp}, a = 0$	44.9(2.9)			
NLO-a^1	$y^{\rm exp}, a = 0$	41.7(4.2)			

Table 4: Hyperfine splittings in the light- and strange-quark sector.

Our result for the hyperfine splitting for the B-system is in good agreement with the experimental value $m_{\rm B^*} - m_{\rm B} = 45.78(35)\,\text{MeV}$ [7], whereas the $\rm B_s$ hyperfine splitting differs noticeably from the experimental value $m_{\rm B_s^*} - m_{\rm B_s} = 48.7^{+2.3}_{-2.1}\,\text{MeV}$. Our results are smaller than the experimental value and than our result for the hyperfine splitting of the B (the opposite of the situation for the experimental values). Since the hyperfine splitting came out far too small in the quenched approximation [34], this is suggestive of a residual quenching effect from the quenching of the strange quark in our $N_{\rm f} = 2$ simulations. Moreover, Fig. 3 indicates larger cutoff effects in the case of the hyperfine splitting for the $\rm B_s$.

3.2 Excited states

For the mass splittings between the ground state $\rm B_q$ and the first excited state, denoted here by $\rm B^r$ and $\rm B_s^r$, we obtain

$$m_{\rm B^r} - m_{\rm B} = 791(73)\,\text{MeV}\,, \qquad [m_{\rm B^r} - m_{\rm B}]^{\rm stat} = 701(65)\,\text{MeV}\,, \tag{3.4a}$$

$$m_{\rm B_s^r} - m_{\rm B_s} = 566(57)\,\text{MeV}\,, \qquad [m_{\rm B_s^r} - m_{\rm B_s}]^{\rm stat} = 547(34)\,\text{MeV}\,. \tag{3.4b}$$

after adding the individually extrapolated results for $[m_{\rm B_q^r} - m_{\rm B_q}]^{\rm stat}$ and $[m_{\rm B_q^r} - m_{\rm B_q}]^{1/\rm m}$. In Fig. 4 these values are shown (as pentagons, slightly shifted at the physical point) for comparison with an extrapolation according to eq. (2.21). The raw data is collected in Tables 5, 6, and 7.

We conclude this Section by remarking that for the excited states the interpretation of our results in terms of mass differences of physical one-meson states, e.g. "radial excitations", is not straight forward. Although our values for these mass gaps are larger than what a multi-hadron state made of, e.g., a $\rm B_{(s)}^{(*)}$-meson and a small number (≤ 2) of physical pions would produce, we cannot unambiguously conclude that our $\rm B_q^r$ states actually correspond to radial excitations of the ground-state $\rm B_q$-mesons. In a rigorous approach,

		$\Delta_{\mathrm{r,d}} m$ [GeV]		$\Delta^{\mathrm{stat}}_{\mathrm{r,d}} m$ [GeV]	
e-id	y	HYP1	HYP2	HYP1	HYP2
A4	0.0771(14)	0.692(37)	0.703(33)	0.619(27)	0.625(25)
A5	0.0624(13)	0.736(18)	0.738(17)	0.655(16)	0.664(15)
B6	0.0484(9)	0.622(66)	0.665(57)	0.552(56)	0.592(52)
E5	0.0926(15)	0.753(27)	0.758(25)	0.676(24)	0.682(23)
F6	0.0562(9)	0.719(57)	0.721(54)	0.658(52)	0.654(47)
F7	0.0449(8)	0.760(32)	0.756(26)	0.678(32)	0.676(30)
G8	0.0260(5)	0.67(11)	0.70(9)	0.63(11)	0.65(9)
N5	0.0940(19)	0.83(11)	0.71(14)	0.697(35)	0.709(31)
N6	0.0662(10)	0.78(9)	0.76(8)	0.634(72)	0.668(58)
O7	0.0447(7)	0.71(12)	0.71(8)	0.64(10)	0.63(8)
LO-a^2	$y^{\mathrm{exp}}, a = 0$	0.787(71)		0.701(65)	
LO-a^1	$y^{\mathrm{exp}}, a = 0$	0.84(12)			

Table 5: Mass gaps between the excited state $\mathrm{B}^{\mathrm{r}}_{\mathrm{d}}$- and the B_{d}-meson at static and next-to-leading order HQET.

		$\Delta_{\mathrm{r,s}} m$ [GeV]		$\Delta^{\mathrm{stat}}_{\mathrm{r,s}} m$ [GeV]	
e-id	y	HYP1	HYP2	HYP1	HYP2
A4	0.0771(14)	0.774(45)	0.748(34)	0.640(23)	0.650(22)
A5	0.0624(13)	0.760(15)	0.753(15)	0.670(11)	0.677(11)
B6	0.0484(9)	0.719(49)	0.704(35)	0.641(22)	0.641(21)
E5	0.0926(15)	0.791(66)	0.676(44)	0.609(29)	0.624(25)
F6	0.0562(9)	0.689(30)	0.722(24)	0.643(18)	0.642(17)
F7	0.0449(8)	0.665(24)	0.660(19)	0.593(15)	0.601(14)
N6	0.0662(10)	0.698(49)	0.718(36)	0.621(38)	0.643(32)
O7	0.0447(7)	–	0.736(38)	–	0.669(29)
LO-a^2	$y^{\mathrm{exp}}, a = 0$	0.570(47)		0.547(34)	
LO-a^1	$y^{\mathrm{exp}}, a = 0$	0.519(74)			

Table 6: Mass gaps between the excited state $\mathrm{B}^{\mathrm{r}}_{\mathrm{s}}$- and the B_{s}-meson at static and next-to-leading order HQET.

		$\Delta^{1/\mathrm{m}}_{\mathrm{r,d}} m$ [MeV]		$\Delta^{1/\mathrm{m}}_{\mathrm{r,s}} m$ [MeV]	
e-id	y	HYP1	HYP2	HYP1	HYP2
A4	0.0771(14)	73(27)	78(21)	133(38)	98(26)
A5	0.0624(13)	71(11)	75(8)	90(11)	76(9)
B6	0.0484(9)	70(31)	73(20)	78(45)	64(28)
E5	0.0926(15)	77(17)	75(9)	182(71)	52(40)
F6	0.0562(9)	61(31)	68(21)	47(24)	80(17)
F7	0.0449(8)	82(18)	80(11)	71(19)	59(15)
G8	0.0260(5)	36(26)	54(15)	–	–
N5	0.0940(19)	132(110)	6(95)	–	–
N6	0.0662(10)	149(59)	94(31)	77(31)	76(18)
O7	0.0447(7)	75(25)	84(17)	–	67(26)
LO-a^1	$y^{\mathrm{exp}}, a = 0$	0.090(40)		0.019(46)	

Table 7: Subleading HQET contributions to the mass gaps between excited and ground states.

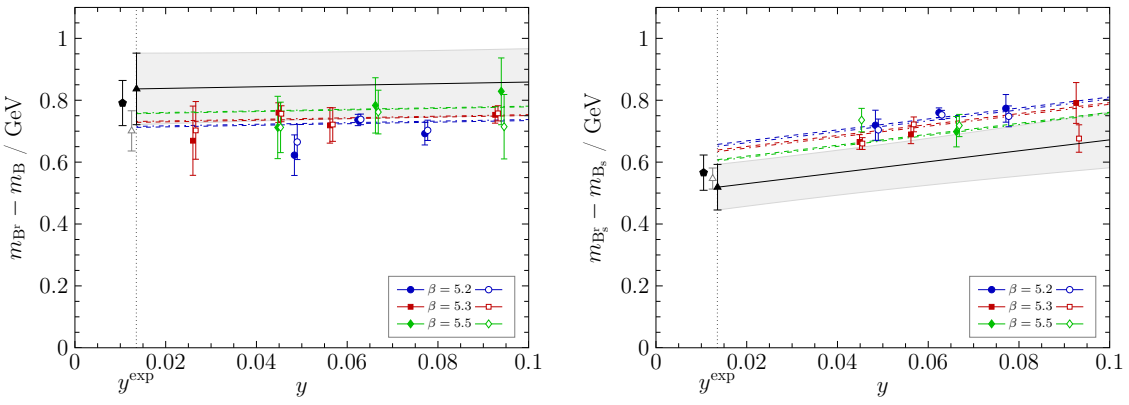

Figure 4: Chiral and continuum extrapolation of $m_{\mathrm{B^r}} - m_{\mathrm{B}}$ (*left*) and $m_{\mathrm{B_s^r}} - m_{\mathrm{B_s}}$ (*right*). Both represent an extrapolation with ansatz (2.21) and $E''_{q,\delta} = 0$ for HQET to order $1/m_{\mathrm{b}}$. The open triangle represents the corresponding result for extrapolating the static order data. For details see Tables 5 and 6. We also add the continuum point (filled black pentagon) corresponding to the combination given in eq. (3.4).

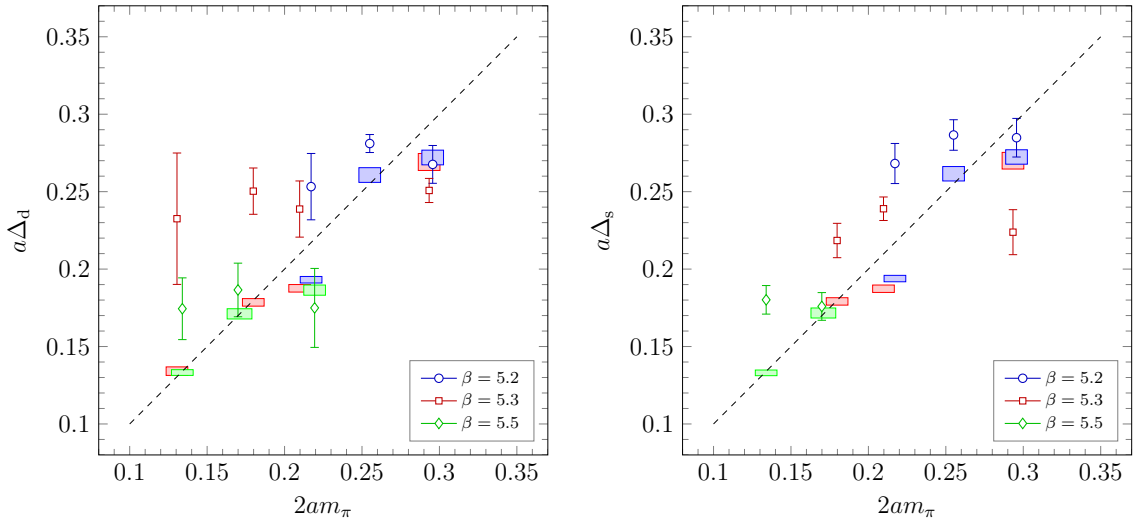

Figure 5: The measured gap $m_{\mathrm{B}_q^{\mathrm{r}}} - m_{\mathrm{B}_q}$ vs. $2m_\pi$ for the excited states $\mathrm{B}_q^{\mathrm{r}}$ with $q = \mathrm{d}$ (*left*) and $q = \mathrm{s}$ (*right*) on each individual CLS ensemble and with HYP2 discretization of the static quark. The boxes are an estimate of the expected gap for a two-hadron state $\mathrm{B}_q^*(-p) + \pi(p)$ with one unit of lattice momentum $p = |\mathbf{p}| = 2\pi/L$. The lower edge of the boxes corresponds to $\Delta_q^{\mathrm{HF}} m + \sqrt{m_\pi^2 + (2\pi/L)^2}$ and the upper edge includes an additional contribution $\mathbf{p}^2/(2m_{\mathrm{B}_q^*})$ as a naive estimate for the kinetic energy of the B_q^*. The dotted line is $\Delta = 2m_\pi$ corresponding to a three-hadron state $\mathrm{B}_q + \pi + \pi$.

states above multi-hadron thresholds need to be treated as resonances in order to obtain precise values for their masses and widths, and to associate them with the states observable in experiments.

Since our lattice study is unquenched, the excited states can also be multi-particle states involving additional pions, beside the desired one-particle state. While it has been argued that the overlap of single-hadron interpolating operators to multi-hadron states is small [41,42], the two-hadron states may have a weaker volume suppression [43]. Moreover, a chiral extrapolation linear in m_π^2 might not be adequate for a multi-hadron state, and a different extrapolation ansatz for these states, e.g. linear in m_π, might also yield somewhat smaller mass gaps.

In continuum (and infinite-volume) physics, any excited B_q-meson state, $\mathrm{B}_q^{\mathrm{x}}$, which strongly decays into an ℓ-wave $\mathrm{B}_q + \pi$ state, i.e. a resonance in the ℓ-wave $\mathrm{B}_q + \pi$ scattering channel, implies that the corresponding two-hadron state $\mathrm{B}_q^{\mathrm{x}} + \pi$ with relative angular momentum ℓ has the correct quantum numbers to couple to our interpolating operators used for the B_q. For the $q = \mathrm{d}$ sector, the set of possible two-hadron excited states includes

- $\mathrm{B}^* + \pi$ in P-wave which would have a non-interacting two-hadron energy gap of $\Delta \gtrsim 181\,\mathrm{MeV}$,
- $\mathrm{B}'^* + \pi$ in P-wave, where B'^* is a radial excitation ($J^P = 1^-$),
- $\mathrm{B}_0^* + \pi$ in S-wave, where B_0^* is an orbital excitation ($J^P = 0^+$),
- $\mathrm{B}_2^* + \pi$ in D-wave, where B_2^* is an orbital excitation ($J^P = 2^+$), like the observed $\mathrm{B}_2^*(5747)^0$ state which would lead to a non-interacting two-hadron energy gap of $\Delta \gtrsim 598\,\mathrm{MeV}$.

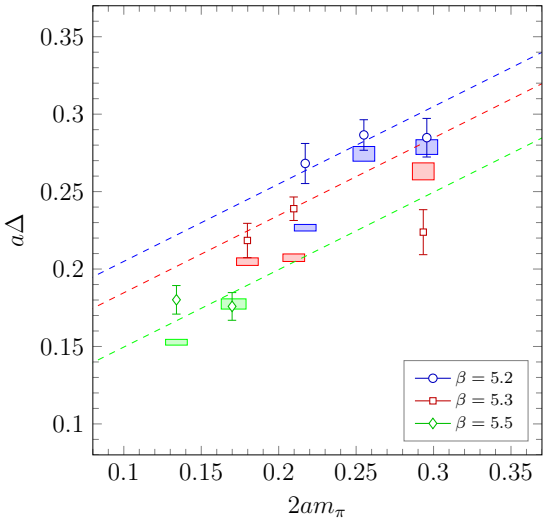

Figure 6: The same data points as in the right panel of Fig. 5 for the measured $\mathrm{B}_\mathrm{s}^\mathrm{r}$ mass gaps, together with estimates of the energy gap for a two-hadron state $\mathrm{B}^*(-p) + \mathrm{K}(p)$ (boxes) and a three-hadron state $\mathrm{B_d} + \mathrm{K} + \pi$ (dashed lines).

On a finite lattice, the energies of states with non-zero relative angular momentum are lifted due to the minimal momentum of $|\mathbf{p}| = 2\pi/L$. Since the s-quark is quenched in our study, we cannot have excited states in the B sector with an s-quark from the sea, like $\mathrm{B}_\mathrm{s}^* + \mathrm{K}$. On the other hand, in the $\mathrm{B_s}$ sector there are two flavour combinations for each of the corresponding excited state of the B sector, e.g. $\mathrm{B}_\mathrm{s}^* + \pi$ and $\mathrm{B}^* + \mathrm{K}$ (corresponding to $\mathrm{B}^* + \pi$).

In Figs. 5 and 6 we show our data points on the various ensembles together with an estimate for the gaps of some two-hadron states. The comparison indicates that some of the two-hadron states can be close in energy to the excited states we measured. Depending on the pion mass on a given ensemble, the energy gaps determined according to eqs. (2.16) may in fact be the energy splitting to the lowest lying $\mathrm{B}^\mathrm{x} + \pi$ state, if this is lighter than the radial excitations B'_q.

Below three- or more-hadron thresholds, the infinite volume scattering matrix (up to corrections which vanish exponentially in the spatial lattice extent) may be inferred from the finite volume energy spectrum [44–48]. In practice this requires the construction of correlation matrices which contain two-hadron as well as single hadron operators. To date, this procedure has been carried out successfully in some simple systems such as $\pi{-}\pi$ and $\pi{-}\mathrm{K}$ scattering, and the energy dependence of the scattering phase shift has been determined with a sufficient resolution to clearly discern resonant behaviour (see e.g. [49] for a recent review). Without performing such a dedicated study, we are not able to conclusively determine the nature of the excited state we observe.

4 Conclusions

In this paper, we have presented results for the B-meson spectrum obtained in the framework of lattice HQET expanded to $\mathrm{O}(1/m_\mathrm{b})$. Within this approach the existence of a continuum limit is guaranteed, as numerically tested with high accuracy in previous studies [50, 51]. In contrast to the HQET expansion in continuum perturbation theory, our

Source ↓	$m_{\mathrm{B_s}}$ 5383(63)	$m_{\mathrm{B}^*} - m_{\mathrm{B}}$ 41.7(4.2)	$m_{\mathrm{B}_\mathrm{s}^*} - m_{\mathrm{B_s}}$ 37.8(3.3)	$m_{\mathrm{B_s}} - m_{\mathrm{B}}$ 88.9(5.7)	$m_{\mathrm{B}^\mathrm{r}} - m_{\mathrm{B}}$ 791(73)	$m_{\mathrm{B}_\mathrm{s}^\mathrm{r}} - m_{\mathrm{B_s}}$ 566(57)
A4	0.46 %	2.52 %	3.51 %	12.48 %	9.79 %	9.93 %
A5	0.30 %	1.32 %	1.81 %	3.14 %	6.67 %	5.78 %
B6	0.03 %	1.50 %	0.39 %	0.23 %	1.04 %	0.06 %
E5	0.28 %	0.40 %	1.80 %	0.46 %	4.72 %	1.51 %
F6	0.10 %	0.34 %	0.45 %	8.62 %	5.07 %	6.72 %
F7	0.21 %	0.82 %	1.50 %	34.56 %	17.87 %	23.42 %
G8	0.53 %	5.25 %	0.00 %	0.05 %	6.46 %	0.03 %
N5	1.90 %	8.04 %	0.45 %	0.01 %	7.94 %	0.05 %
N6	5.97 %	1.33 %	29.18 %	31.56 %	14.60 %	27.70 %
O7	4.50 %	6.34 %	13.49 %	8.05 %	25.32 %	14.42 %
ω	62.84 %	31.75 %	46.61 %	0.04 %	0.09 %	0.05 %
Z_{A}	21.13 %	0.27 %	0.63 %	0.75 %	0.40 %	0.19 %

Table 8: Distributions of relative squared errors, $\sigma_i^2 / \sum_j \sigma_j^2$ among different sources i for the mean values given in (3.1)-(3.4). In the second row we repeat them in MeV for the reader's convenience, including only the statistical error of the mean. Remaining relative errors enter through the scale setting procedure only.

approach is manifestly non-perturbative in the strong coupling. We perform the continuum extrapolation from lattice resolutions in the range 0.08–0.05 fm. Pion masses, in our setup with $N_{\mathrm{f}} = 2$ degenerate flavours, reach down to values of about 190 MeV. The accuracy is at the 10% level, for the different splittings presented (e.g., hyperfine and $\mathrm{B_d}$–$\mathrm{B_s}$ splittings), and we always find consistency within two standard deviations with values from the PDG, whenever a comparison is possible.

Hyperfine splittings probe higher-order terms in HQET and the reported results represent an important check on the validity and the reliability of the asymptotic HQET expansion, truncated at NLO, at the b-quark mass scale. Compared to previous quenched results, we observe a significant shift for the hyperfine splitting in the B-meson sector, which now agrees with the experimental determination. In our $N_{\mathrm{f}} = 2$ simulations, the hyperfine splitting in the $\mathrm{B_s}$ sector appears to suffer from a residual quenching effect, which is in line with what was seen for $N_{\mathrm{f}} = 0$. In order to ascertain that the quenching of the strange quark is indeed the root cause of the reduced $\mathrm{B_s}$ hyperfine splitting seen here, we plan to extend our computations to simulations of the $N_{\mathrm{f}} = 2 + 1$ theory [52].

A dominant source of uncertainty in our results is represented by cutoff effects (see Tab. 8). This does not come unexpected since we have not implemented $\mathrm{O}(a)$ improvement at $\mathrm{O}(1/m_{\mathrm{b}})$. While implementing a fully non-perturbative improvement programme at this order is probably too difficult, one may consider perturbative (tree level or one-loop) improvement for future applications.

We also determined the mass gaps for excited states in both the B and the $\mathrm{B_s}$ sectors. The results are consistent with a radial splitting, e.g. as computed for the $\mathrm{B_c}$ system in [6], but these excited states might also be two- or multi-hadron states.

Knowledge of the mass splittings is relevant for the computation of hadronic parameters within the sum-rules approach and when comparing results from the lattice to sum-rules estimates. The mass gaps of excited states are also an important information for the computation of form-factors on the lattice, for example for the $\mathrm{B} \to \pi\ell\nu$ and the

$B_s \to K\ell\nu$ decays, as currently endeavored by the ALPHA Collaboration [53, 54], and in general in the spectral analysis of two- and three-point functions.

Acknowledgements. We like to thank R. Sommer for many helpful discussions and contributions to the study presented here, and we thank our colleagues in the CLS effort for the joint production and use of gauge configurations. We acknowledge partial support by the SFB/TR 9, by grant HE 4517/2-1 (P.F. and J.H.) and HE 4517/3-1 (J.H.) of the Deutsche Forschungsgemeinschaft, by the European Community through EU Contract MRTN-CT-2006-035482, "FLAVIAnet", by the Spanish Minister of Education and Science projects RyC-2011-08557 and by the Danish National Research Foundation under the grant n. DNRF:90 (M.D.M.). P.F. acknowledges financial support from the Spanish MINECO under grants FPA2012-31880 and SEV-2012-0249 ("Centro de Excelencia Severo Ochoa" Programme).

We gratefully acknowledge the computer resources granted by the John von Neumann Institute for Computing (NIC) and provided on the supercomputer JUROPA at Jülich Supercomputing Centre (JSC) and by the Gauss Centre for Supercomputing (GCS) through the NIC on the GCS share of the supercomputer JUQUEEN at JSC, with funding by the German Federal Ministry of Education and Research (BMBF) and the German State Ministries for Research of Baden-Württemberg (MWK), Bayern (StMWFK) and Nordrhein-Westfalen (MIWF), as well as within the Distributed European Computing Initiative by the PRACE-2IP, with funding from the European Community's Seventh Framework Programme (FP7/2007-2013) under grant agreement RI-283493, by the Grand Équipement National de Calcul Intensif at CINES in Montpellier under the allocation 2012-056808, by the HLRN in Berlin, and by NIC at DESY, Zeuthen.

A Determination of the statistical error in the presence of autocorrelations

In order to compute the statistical error in the presence of both correlations between the different observables and of autocorrelations along the HMC trajectories by which our ensembles were generated, we employ the methods of [55–58], which we briefly outline below.

The starting point is the computation of the "primary" observables C^i_α, where i labels the N_{meas} gauge configurations, and α is an aggregate label for the different correlators measured (stat, spin, kin), the Euclidean time separation t between the source and sink, and the different smearing levels employed at source and sink. The gauge average $\overline{C}_\alpha$ and the variance $\sigma^2_{C_\alpha}$ are computed as usual. To estimate the true statistical error $\sigma_{\overline{C}_\alpha}$ of the gauge average, we also require the integrated autocorrelation time $\tau^{\mathrm{int}}_{C_\alpha}$, which is computed from the autocorrelation function

$$\Gamma^{(1)}_{\alpha\beta} \equiv \Gamma_{C_\alpha C_\beta}(\tau) = \lim_{K\to\infty} \frac{1}{K} \sum_{i=1}^{K} \left(C^{i+\tau}_\alpha - \overline{C}_\alpha\right)\left(C^i_\beta - \overline{C}_\beta\right) , \tag{A.1}$$

where τ is the separation in simulation time along the Markov chain. In order to take into account the long-time tail of Γ, the conservative estimate [56]

$$\tau^{\mathrm{int}}_{C_\alpha} = \frac{1}{2} + \frac{1}{\Gamma^{(1)}_{\alpha\alpha}(0)} \left(\sum_{\tau=1}^{W-1} \Gamma^{(1)}_{\alpha\alpha}(\tau) + \tau^{\mathrm{exp}} \Gamma^{(1)}_{\alpha\alpha}(W) \right) \tag{A.2}$$

is used, where τ^{exp} is an estimate of the exponential autocorrelation time of the Markov chain. The values used in our analysis are listed in Table 2. The window size W is

automatically chosen as the point $\tau = W$ where $\Gamma_{\alpha\alpha}(\tau)$ comes close to zero within about 1.5 of its estimated error. The true statistical error is then given by

$$\sigma^2_{\overline{C}_\alpha} = 2\tau^{\mathrm{int}}_{C_\alpha} \frac{\sigma^2_{C_\alpha}}{N_{\mathrm{meas}}} \,. \tag{A.3}$$

For derived observables $D_{\alpha'}$, which are functions of gauge averages of the primary observables $\overline{C}_\alpha$, and in our case include the generalized eigenvalues and eigenvectors as well as the energies derived from them, we compute the derivatives

$$J_{\alpha'\alpha} \equiv \frac{\partial D_{\alpha'}}{\partial \overline{C}_\alpha} \tag{A.4}$$

and the autocorrelation function [56]

$$\Gamma^{(2)}_{\alpha'\beta'}(\tau) \equiv \sum_{\alpha,\beta} J_{\alpha'\alpha} \Gamma^{(1)}_{\alpha\beta}(\tau) J_{\beta'\beta} \,. \tag{A.5}$$

The variance of the derived observable $D_{\alpha'}$ is then given by

$$\sigma^2_{D_{\alpha'}} = \Gamma^{(2)}_{\alpha'\alpha'}(0) \tag{A.6}$$

and its statistical error by

$$\sigma^2_{\overline{D}'_\alpha} = 2\tau^{\mathrm{int}}_{D'_\alpha} \frac{\sigma^2_{D'_\alpha}}{N_{\mathrm{meas}}} \,, \tag{A.7}$$

where the integrated autocorrelation time $\tau^{\mathrm{int}}_{D'_\alpha}$ is again estimated using (A.2), with $\Gamma^{(2)}$ substituted for $\Gamma^{(1)}$.

Since the extraction of plateau values from a weighted fit requires knowledge of the errors of the individual points, in principle this procedure should be iterated, with the plateau averages as secondary derived observables of the derived observables. However, the integrated autocorrelation times for the effective energies in the plateau region do not markedly differ. Therefor, it is sufficient to employ their variances (as estimated using e.g. a Jackknife procedure for error propagation) to weight the fit, treating only the fitted values as derived observables. This simplified procedure has been adopted here.

In order to extract the final answer in physical units, the plateau values must be combined with each other and with the HQET parameters and lattice spacing, propagating the errors on each of those to the final result, where the HQET parameters are statistically independent of the large-volume observables; similarly, in extrapolating to the chiral and continuum limits, the results obtained from different ensembles are statistically independent, and their contribution to the error of the final result f can thus be added in quadrature:

$$\sigma^2_f = \sum_e \sigma^2_f(e) + \sum_{i,j} \frac{\partial f}{\partial Y_i} C_{Y_i Y_j} \frac{\partial f}{\partial Y_j} \,, \tag{A.8}$$

where the Y_i are the additional parameters, $C_{Y_i Y_j}$ is their (known) covariance matrix, and $\sigma^2_f(e)$ is the error computed according to eqn. (A.7) when taking into account only the fluctuations of C_α on ensemble e [56–58].

	$aE^{\rm stat}_{n=1}$		$a^2E^{\rm kin}_{n=1}$		$-a^2E^{\rm spin}_{n=1}$	
e-id	HYP1	HYP2	HYP1	HYP2	HYP1	HYP2
A4	$0.4193(5)_{11}$	$0.3841(4)_{11}$	$0.8538(9)_{8}$	$0.8987(6)_{8}$	$0.02281(16)_{7}$	$0.02183(13)_{7}$
A5c	$0.4151(5)_{10}$	$0.3802(4)_{10}$	$0.8520(6)_{7}$	$0.8962(4)_{7}$	$0.02253(18)_{7}$	$0.02154(14)_{7}$
A5d	$0.4143(6)_{10}$	$0.3791(5)_{10}$	$0.8510(9)_{7}$	$0.8961(6)_{7}$	$0.02210(24)_{7}$	$0.02105(20)_{7}$
B6	$0.4069(10)_{11}$	$0.3716(8)_{11}$	$0.8490(10)_{7}$	$0.8946(7)_{7}$	$0.02187(29)_{7}$	$0.02067(22)_{7}$
E5	$0.3845(4)_{12}$	$0.3511(4)_{12}$	$0.8115(9)_{9}$	$0.8523(6)_{9}$	$0.01762(19)_{9}$	$0.01675(15)_{9}$
F6	$0.3727(10)_{13}$	$0.3392(8)_{13}$	$0.8089(15)_{9}$	$0.8490(9)_{9}$	$0.01697(33)_{9}$	$0.01632(24)_{9}$
F7	$0.3700(11)_{13}$	$0.3354(9)_{13}$	$0.8087(15)_{9}$	$0.8486(9)_{9}$	$0.01563(33)_{9}$	$0.01519(24)_{9}$
G8	$0.3672(13)_{11}$	$0.3327(11)_{11}$	$0.8044(27)_{9}$	$0.8470(16)_{9}$	$0.01633(57)_{9}$	$0.01508(38)_{9}$
N5	$0.3195(5)_{16}$	$0.2885(5)_{16}$	$0.7414(15)_{12}$	$0.7749(9)_{12}$	$0.01018(25)_{12}$	$0.00973(18)_{12}$
N6	$0.3129(9)_{16}$	$0.2825(6)_{16}$	$0.7423(19)_{12}$	$0.7727(11)_{12}$	$0.00989(33)_{12}$	$0.00899(21)_{12}$
O7	$0.3093(10)_{16}$	$0.2785(8)_{16}$	$0.7389(26)_{12}$	$0.7746(14)_{12}$	$0.01000(42)_{12}$	$0.00916(28)_{12}$

Table 9: Raw data for plateau-averaged ground state energies in the heavy-light sector. The subscript to the statistical error is the value of $t_{\rm min}$ in the GEVP analysis.

B Effective energies and matrix elements

In this Appendix we provide the numerical results of our GEVP analysis after performing a weighted plateaux average

$$E_n^{\rm x} = \frac{\sum_t w(t) E_n^{\rm eff,x}(t,t_0)}{\sum_t w(t)}\,, \qquad\qquad w(t) = \Big(\sigma\big[E_n^{\rm eff,x}(t,t_0)\big]\Big)^{-2} \tag{B.1}$$

for $t \in [t_{\rm min}, t_{\rm max}]$ and $t_0 \geq t_{\rm min}/2$, see Section 2.2. The specific value of $t_{\rm max}$ is irrelevant due to noise dominated data at large time separations.[2] As a consequence of the exponential growth of the noise-to-signal ratio, the quoted errors are dominated by the error at $t_{\rm min}$ and we decided to quote $t_{\rm min}$ as subscript to the statistical error in the following Tables. For determining $t_{\rm min}$, we use $t_0 = t - 1$ in the GEVP, and then $t_0 = t_{\rm min} - 1$ once $t_{\rm min}$ is fixed. The errors quoted are those entering the corresponding effective energy plots presented below and do not contain the tail contribution of the error. Since the autocorrelation is expected to be the same among different time slices in the plateau region, it does not affect the estimate (B.1) and can be added, including the exponential tail, whenever needed explicitly. In fact, all values quoted for derived observables as presented in the main text have the exponential tail included as discussed in Appendix A.

The same procedure has been used to obtain matrix elements $p^{\rm x}$. We include them in the present paper (Table 13-14) in order to complete the data set used in [10, 36].

A special case is the ensemble labeled A5 for which we have two independent Monte Carlo histories/replicas (A5c and A5d). Here, measurements and a subsequent GEVP analysis have been independently performed for both replicas in the heavy-light sector but only on A5d for heavy-strange. The results from different replicas are then combined before derived observables as presented in the main text are computed.

[2] For plotting convenience we set $t_{\rm max}/a = \infty$ in the plots.

	$aE^{\rm stat}_{n=2}$		$a^2E^{\rm kin}_{n=2}$		$-a^2E^{\rm spin}_{n=2}$	
e-id	HYP1	HYP2	HYP1	HYP2	HYP1	HYP2
A4	$0.655(9)_{10}$	$0.622(8)_{10}$	$0.931(22)_{9}$	$0.975(16)_{9}$	$0.0249(14)_{7}$	$0.0210(12)_{7}$
A5c	$0.668(5)_{9}$	$0.633(4)_{9}$	$0.926(10)_{8}$	$0.969(7)_{8}$	$0.0246(7)_{6}$	$0.0213(6)_{6}$
A5d	$0.668(8)_{9}$	$0.631(7)_{9}$	$0.932(16)_{8}$	$0.977(11)_{8}$	$0.0268(11)_{6}$	$0.0234(9)_{6}$
B6	$0.617(17)_{10}$	$0.597(16)_{10}$	$0.926(20)_{8}$	$0.970(14)_{8}$	$0.0256(14)_{6}$	$0.0218(11)_{6}$
E5	$0.608(7)_{11}$	$0.577(6)_{11}$	$0.878(10)_{9}$	$0.915(6)_{9}$	$0.0204(13)_{8}$	$0.0182(10)_{8}$
F6	$0.590(13)_{11}$	$0.556(12)_{11}$	$0.862(17)_{9}$	$0.901(11)_{9}$	$0.0192(23)_{8}$	$0.0157(18)_{8}$
F7	$0.594(12)_{11}$	$0.559(11)_{11}$	$0.859(15)_{9}$	$0.902(10)_{9}$	$0.0072(67)_{10}$	$0.0104(49)_{10}$
G8	$0.577(27)_{11}$	$0.548(23)_{11}$	$0.853(13)_{8}$	$0.906(9)_{8}$	$0.0277(36)_{8}$	$0.0230(28)_{8}$
N5	$0.490(5)_{13}$	$0.462(4)_{13}$	$0.805(30)_{13}$	$0.779(17)_{13}$	$0.0112(11)_{10}$	$0.0103(8)_{10}$
N6	$0.468(14)_{15}$	$0.446(11)_{15}$	$0.815(19)_{12}$	$0.822(12)_{12}$	$0.0113(14)_{10}$	$0.0116(10)_{10}$
O7	$0.465(17)_{14}$	$0.432(13)_{14}$	$0.777(8)_{10}$	$0.815(5)_{10}$	$0.0118(17)_{10}$	$0.0096(13)_{10}$

Table 10: Raw data for plateau-averaged 1$^{\rm st}$ excited state energies in the heavy-light sector. The subscript to the statistical error is the value of $t_{\rm min}$ in the GEVP analysis.

	$aE^{\rm stat}_{n=1}$		$a^2E^{\rm kin}_{n=1}$		$-a^2E^{\rm spin}_{n=1}$	
e-id	HYP1	HYP2	HYP1	HYP2	HYP1	HYP2
A4	$0.43905(46)_{10}$	$0.40430(40)_{10}$	$0.8585(8)_{7}$	$0.9024(5)_{7}$	$0.02365(22)_{7}$	$0.02220(17)_{7}$
A5c	$0.43856(53)_{9}$	$0.40378(46)_{9}$	$0.8590(11)_{7}$	$0.9006(7)_{7}$	$0.02308(29)_{7}$	$0.02214(24)_{7}$
B6	$0.43224(41)_{12}$	$0.39722(32)_{12}$	$0.8556(4)_{7}$	$0.8990(3)_{7}$	$0.02273(11)_{7}$	$0.02139(9)_{7}$
E5	$0.40063(44)_{12}$	$0.36736(36)_{12}$	$0.8157(11)_{9}$	$0.8561(7)_{9}$	$0.01820(31)_{10}$	$0.01753(21)_{10}$
F6	$0.39468(35)_{14}$	$0.36063(27)_{14}$	$0.8122(6)_{9}$	$0.8530(4)_{9}$	$0.01683(12)_{9}$	$0.01612(9)_{9}$
F7	$0.39217(66)_{14}$	$0.35837(54)_{14}$	$0.8118(11)_{9}$	$0.8534(7)_{9}$	$0.01627(22)_{9}$	$0.01576(16)_{9}$
N6	$0.32827(44)_{17}$	$0.29799(33)_{17}$	$0.7429(11)_{12}$	$0.7758(6)_{12}$	$0.00991(18)_{12}$	$0.00941(12)_{12}$
O7	–	$0.29571(34)_{16}$	–	$0.7753(8)_{12}$	–	$0.00905(15)_{12}$

Table 11: Raw data for plateau-averaged ground state energies in the heavy-strange sector. The subscript to the statistical error is the value of $t_{\rm min}$ in the GEVP analysis.

References

[1] **HPQCD** Collaboration, T. C. Hammant, A. G. Hart, G. M. von Hippel, R. R. Horgan, and C. J. Monahan, *Radiative improvement of the lattice NRQCD action using the background field method and application to the hyperfine splitting of quarkonium states*, *Phys.Rev.Lett.* **107** (2011) 112002, [arXiv:1105.5309].

[2] T. Hammant, A. Hart, G. von Hippel, R. Horgan, and C. Monahan, *Radiative improvement of the lattice NRQCD action using the background field method with applications to quarkonium spectroscopy*, *Phys.Rev.* **D88** (2013) 014505, [arXiv:1303.3234].

[3] **HPQCD** Collaboration, R. Dowdall, C. Davies, T. Hammant, and R. Horgan, *Bottomonium hyperfine splittings from lattice NRQCD including radiative and relativistic corrections*, *Phys.Rev.* **D89** (2014), no. 3 031502, [arXiv:1309.5797].

[4] **HPQCD** Collaboration, C. Davies, E. Follana, I. Kendall, G. P. Lepage, and C. McNeile, *Precise determination of the lattice spacing in full lattice QCD*, *Phys.Rev.* **D81** (2010) 034506, [arXiv:0910.1229].

	$aE^{\rm stat}_{n=1}$		$a^2E^{\rm kin}_{n=1}$		$-a^2E^{\rm spin}_{n=1}$	
e-id	HYP1	HYP2	HYP1	HYP2	HYP1	HYP2
A4	$0.6829(77)_9$	$0.6519(69)_9$	$0.995(35)_9$	$0.999(23)_9$	$0.0250(12)_6$	$0.0217(10)_6$
A5c	$0.6936(63)_8$	$0.6614(58)_8$	$0.952(20)_8$	$0.975(15)_8$	$0.0243(16)_6$	$0.0212(13)_6$
B6	$0.6762(61)_{10}$	$0.6411(54)_{10}$	$0.934(33)_{10}$	$0.960(21)_{10}$	$0.0224(11)_7$	$0.0201(9)_7$
E5	$0.6022(82)_{11}$	$0.5740(73)_{11}$	$0.959(47)_{11}$	$0.894(30)_{11}$	$0.0170(17)_8$	$0.0162(13)_8$
F6	$0.6074(42)_{11}$	$0.5730(37)_{11}$	$0.855(13)_{10}$	$0.914(8)_{10}$	$0.0199(26)_{10}$	$0.0147(18)_{10}$
F7	$0.5885(68)_{11}$	$0.5573(62)_{11}$	$0.873(22)_{10}$	$0.902(13)_{10}$	$0.0186(16)_8$	$0.0167(12)_8$
N6	$0.4803(75)_{15}$	$0.4554(58)_{15}$	$0.781(12)_{12}$	$0.813(7)_{12}$	$0.0107(8)_{10}$	$0.0105(6)_{10}$
O7	–	$0.4594(49)_{14}$	–	$0.807(9)_{12}$	–	$0.0091(12)_{11}$

Table 12: Raw data for plateau-averaged 1st excited state energies in the heavy-strange sector. The subscript to the statistical error is the value of $t_{\rm min}$ in the GEVP analysis.

[5] **HPQCD** Collaboration, R. Dowdall et al., *The Upsilon spectrum and the determination of the lattice spacing from lattice QCD including charm quarks in the sea*, *Phys.Rev.* **D85** (2012) 054509, [arXiv:1110.6887].

[6] R. Dowdall, C. Davies, T. Hammant, and R. Horgan, *Precise heavy-light meson masses and hyperfine splittings from lattice QCD including charm quarks in the sea*, *Phys.Rev.* **D86** (2012) 094510, [arXiv:1207.5149].

[7] **Particle Data Group** Collaboration, K. Olive et al., *Review of Particle Physics*, *Chin.Phys.* **C38** (2014) 090001.

[8] E. Eichten and B. R. Hill, *Static Effective Field Theory: $1/m$ Corrections*, *Phys.Lett.* **B243** (1990) 427.

[9] M. Neubert, *Heavy quark symmetry*, *Phys.Rept.* **245** (1994) 259, [hep-ph/9306320].

[10] **ALPHA** Collaboration, F. Bernardoni et al., *The b-quark mass from non-perturbative $N_f = 2$ Heavy Quark Effective Theory at $O(1/m_h)$*, *Phys.Lett.* **B730** (2014) 171, [arXiv:1311.5498].

[11] **CDF** Collaboration, T. A. Aaltonen et al., *Study of orbitally excited B mesons and evidence for a new $B\pi$ resonance*, *Phys.Rev.* **D90** (2014), no. 1 012013, [arXiv:1309.5961].

[12] S. Collins, C. Davies, U. M. Heller, A. Ali Khan, J. Shigemitsu, et al., *Sea quark effects in B spectroscopy and decay constants*, *Phys.Rev.* **D60** (1999) 074504, [hep-lat/9901001].

[13] E. B. Gregory, C. T. Davies, I. D. Kendall, J. Koponen, K. Wong, et al., *Precise B, B_s and B_c meson spectroscopy from full lattice QCD*, *Phys.Rev.* **D83** (2011) 014506, [arXiv:1010.3848].

[14] **UKQCD** Collaboration, C. Michael and J. Peisa, *Maximal variance reduction for stochastic propagators with applications to the static quark spectrum*, *Phys.Rev.* **D58** (1998) 034506, [hep-lat/9802015].

[15] **UKQCD** Collaboration, A. M. Green, J. Koponen, C. McNeile, C. Michael, and G. Thompson, *Excited B mesons from the lattice*, *Phys.Rev.* **D69** (2004) 094505, [hep-lat/0312007].

[16] T. Burch and C. Hagen, *Domain decomposition improvement of quark propagator estimation*, *Comput.Phys.Commun.* **176** (2007) 137, [hep-lat/0607029].

[17] J. Foley, A. O'Cais, M. Peardon, and S. M. Ryan, *Radial and orbital excitations of static-light mesons*, *Phys.Rev.* **D75** (2007) 094503, [hep-lat/0702010].

	$a^{3/2}p^{\rm stat}_{n=1}$		$-ap^{\rm kin}_{n=1}$	
e-id	HYP1	HYP2	HYP1	HYP2
A4	$0.1223(5)_{10}$	$0.1036(4)_{10}$	$1.482(37)_{8}$	$0.727(35)_{8}$
A5c	$0.1205(4)_{9}$	$0.1018(3)_{9}$	$1.501(19)_{6}$	$0.748(19)_{6}$
A5d	$0.1192(6)_{9}$	$0.1012(5)_{9}$	$1.503(26)_{6}$	$0.749(26)_{6}$
B6	$0.1144(13)_{11}$	$0.0970(10)_{11}$	$1.473(44)_{7}$	$0.743(41)_{7}$
E5	$0.0984(4)_{11}$	$0.0849(3)_{11}$	$1.360(30)_{8}$	$0.703(30)_{8}$
F6	$0.0918(10)_{12}$	$0.0787(8)_{12}$	$1.329(49)_{8}$	$0.668(45)_{8}$
F7	$0.0896(9)_{12}$	$0.0776(7)_{12}$	$1.299(52)_{8}$	$0.654(48)_{8}$
G8	$0.0870(13)_{11}$	$0.0755(10)_{11}$	$1.370(56)_{7}$	$0.703(52)_{7}$
N5	$0.0620(6)_{15}$	$0.0555(5)_{15}$	$1.126(40)_{9}$	$0.615(37)_{9}$
N6	$0.0580(11)_{16}$	$0.0510(7)_{16}$	$1.145(69)_{10}$	$0.599(61)_{10}$
O7	$0.0559(13)_{16}$	$0.0490(9)_{16}$	$1.134(62)_{9}$	$0.617(56)_{9}$
	$ap^{\rm A_0^{(1)}}_{n=1}$		$ap^{\rm spin}_{n=1}$	
e-id	HYP1	HYP2	HYP1	HYP2
A4	$0.4451(9)_{11}$	$0.3970(7)_{11}$	$0.4792(5)_{5}$	$0.4504(5)_{5}$
A5c	$0.4450(5)_{9}$	$0.3975(4)_{9}$	$0.4637(2)_{3}$	$0.4385(2)_{3}$
A5d	$0.4440(14)_{9}$	$0.3952(6)_{9}$	$0.4639(3)_{3}$	$0.4385(3)_{3}$
B6	$0.4422(13)_{10}$	$0.3951(10)_{10}$	$0.4793(10)_{5}$	$0.4505(9)_{5}$
E5	$0.4149(9)_{12}$	$0.3677(6)_{12}$	$0.4663(7)_{6}$	$0.4393(7)_{6}$
F6	$0.4121(17)_{12}$	$0.3664(12)_{12}$	$0.4673(11)_{6}$	$0.4414(10)_{6}$
F7	$0.4123(18)_{12}$	$0.3645(12)_{12}$	$0.4680(11)_{6}$	$0.4426(11)_{6}$
G8	$0.4111(21)_{11}$	$0.3629(16)_{11}$	$0.4698(19)_{6}$	$0.4412(18)_{6}$
N5	$0.3674(12)_{14}$	$0.3207(8)_{14}$	$0.4361(14)_{8}$	$0.4149(13)_{8}$
N6	$0.3583(20)_{15}$	$0.3171(13)_{15}$	$0.4351(16)_{8}$	$0.4169(14)_{8}$
O7	$0.3645(21)_{14}$	$0.3200(13)_{14}$	$0.4362(22)_{8}$	$0.4139(18)_{8}$

Table 13: Raw data for plateau-averaged ground state matrix elements in the heavy-light sector. The subscript to the statistical error is the value of $t_{\rm min}$ in the GEVP analysis.

[18] **UKQCD** Collaboration, J. Koponen, *Energies of B_s meson excited states: A Lattice study*, *Phys.Rev.* **D78** (2008) 074509, [arXiv:0708.2807].

[19] J. Koponen, *Energies and radial distributions of B_s mesons on the lattice*, *Acta Phys.Polon.* **B38** (2007) 2893, [hep-lat/0702006].

[20] T. Burch, C. Hagen, C. B. Lang, M. Limmer, and A. Schäfer, *Excitations of single-beauty hadrons*, *Phys.Rev.* **D79** (2009) 014504, [arXiv:0809.1103].

[21] **ETM** Collaboration, K. Jansen, C. Michael, A. Shindler, and M. Wagner, *The static-light meson spectrum from twisted mass lattice QCD*, *JHEP* **0812** (2008) 058, [arXiv:0810.1843].

[22] **ETM** Collaboration, C. Michael, A. Shindler, and M. Wagner, *The continuum limit of the static-light meson spectrum*, *JHEP* **1008** (2010) 009, [arXiv:1004.4235].

[23] **ALPHA** Collaboration, B. Blossier et al., *Parameters of Heavy Quark Effective Theory from $N_f = 2$ lattice QCD*, *JHEP* **1209** (2012) 132, [arXiv:1203.6516].

[24] **ALPHA** Collaboration, M. Della Morte, A. Shindler, and R. Sommer, *On lattice actions for static quarks*, *JHEP* **08** (2005) 051, [hep-lat/0506008].

	$a^{3/2}p^{\rm stat}_{n=1}$		$-ap^{\rm kin}_{n=1}$	
e-id	HYP1	HYP2	HYP1	HYP2
A4	$0.13448(77)_{10}$	$0.11329(58)_{10}$	$1.553(37)_{7}$	$0.757(36)_{7}$
A5	$0.13457(78)_{9}$	$0.11269(60)_{9}$	$1.563(34)_{6}$	$0.781(33)_{6}$
B6	$0.13143(50)_{11}$	$0.11041(37)_{11}$	$1.536(31)_{8}$	$0.747(29)_{8}$
E5	$0.10746(71)_{12}$	$0.09264(51)_{12}$	$1.391(41)_{8}$	$0.712(39)_{8}$
F6	$0.10521(47)_{13}$	$0.09019(34)_{13}$	$1.387(35)_{9}$	$0.689(31)_{9}$
F7	$0.10296(82)_{13}$	$0.08857(61)_{13}$	$1.403(38)_{8}$	$0.703(38)_{8}$
N6	$0.06562(56)_{16}$	$0.05788(40)_{16}$	$1.173(46)_{10}$	$0.611(41)_{10}$
O7	–	$0.05745(48)_{15}$	–	$0.620(39)_{9}$
	$ap^{\mathrm{A}_0^{(1)}}_{n=1}$		$ap^{\rm spin}_{n=1}$	
e-id	HYP1	HYP2	HYP1	HYP2
A4	$0.4426(9)_{10}$	$0.39451(72)_{10}$	$0.4778(9)_{5}$	$0.4488(9)_{5}$
A5c	$0.4395(10)_{9}$	$0.39354(72)_{9}$	$0.4782(13)_{5}$	$0.4493(12)_{5}$
B6	$0.4374(8)_{12}$	$0.39070(61)_{12}$	$0.4799(5)_{5}$	$0.4505(5)_{5}$
E5	$0.4164(10)_{12}$	$0.36767(78)_{12}$	$0.4657(10)_{6}$	$0.4393(9)_{6}$
F6	$0.4117(6)_{12}$	$0.36459(42)_{12}$	$0.4658(6)_{6}$	$0.4398(5)_{6}$
F7	$0.4094(12)_{13}$	$0.36180(93)_{13}$	$0.4670(10)_{6}$	$0.4395(8)_{6}$
N6	$0.3605(13)_{16}$	$0.31679(90)_{16}$	$0.4364(10)_{8}$	$0.4165(9)_{8}$
O7	–	$0.31636(88)_{15}$	–	$0.4176(13)_{8}$

Table 14: Raw data for plateau-averaged ground state matrix elements in the heavy-strange sector.

[25] B. Berg and A. Billoire, *Glueball Spectroscopy in Four-Dimensional SU(3) Lattice Gauge Theory. 1.*, *Nucl.Phys.* **B221** (1983) 109.

[26] L. Griffiths, C. Michael, and P. E. Rakow, *Mesons With Excited Glue*, *Phys.Lett.* **B129** (1983) 351.

[27] C. Michael and I. Teasdale, *Extracting Glueball Masses From Lattice QCD*, *Nucl.Phys.* **B215** (1983) 433.

[28] C. Michael, *Adjoint Sources in Lattice Gauge Theory*, *Nucl.Phys.* **B259** (1985) 58.

[29] M. Lüscher and U. Wolff, *How to calculate the elastic scattering matrix in two-dimensional quantum field theories by numerical simulation*, *Nucl.Phys.* **B339** (1990) 222.

[30] **ALPHA** Collaboration, B. Blossier, M. Della Morte, G. von Hippel, T. Mendes, and R. Sommer, *On the generalized eigenvalue method for energies and matrix elements in lattice field theory*, *JHEP* **0904** (2009) 094, [arXiv:0902.1265].

[31] S. Güsken et al., *Nonsinglet axial vector couplings of the baryon octet in lattice QCD*, *Phys. Lett.* **B227** (1989) 266.

[32] **APE** Collaboration, M. Albanese et al., *Glueball masses and string tension in lattice QCD*, *Phys. Lett.* **192B** (1987) 163.

[33] S. Basak et al., *Combining Quark and Link Smearing to Improve Extended Baryon Operators*, *PoS* **LAT2005** (2006) 076, [hep-lat/0509179].

[34] **ALPHA** Collaboration, B. Blossier et al., *HQET at order $1/m$: II. Spectroscopy in the quenched approximation*, *JHEP* **1005** (2010) 074, [arXiv:1004.2661].

[35] **ALPHA** Collaboration, B. Blossier et al., *HQET at order 1/m: III. Decay constants in the quenched approximation*, *JHEP* **1012** (2010) 039, [arXiv:1006.5816].

[36] **ALPHA** Collaboration, F. Bernardoni, B. Blossier, J. Bulava, M. Della Morte, P. Fritzsch, et al., *Decay constants of B-mesons from non-perturbative HQET with two light dynamical quarks*, *Phys.Lett.* **B735** (2014), no. 0 349, [arXiv:1404.3590].

[37] **ALPHA** Collaboration, P. Fritzsch et al., *The strange quark mass and Lambda parameter of two flavor QCD*, *Nucl.Phys.* **B865** (2012) 397, [arXiv:1205.5380].

[38] F. Bernardoni, P. Hernández, and S. Necco, *Heavy-light mesons in the ϵ-regime*, *JHEP* **1001** (2010) 070, [arXiv:0910.2537].

[39] **ALPHA** Collaboration, F. Bernardoni, J. Bulava, M. Donnellan, and R. Sommer, *Precision lattice QCD computation of the $B^*B\pi$ coupling*, *Phys.Lett.* **B740** (2014) 278, [arXiv:1404.6951].

[40] E. E. Jenkins, *Heavy meson masses in chiral perturbation theory with heavy quark symmetry*, *Nucl.Phys.* **B412** (1994) 181, [hep-ph/9212295].

[41] C. Michael, *Hadronic decays*, *PoS* **LAT2005** (2006) 008, [hep-lat/0509023].

[42] O. Bär and M. Golterman, *Excited-state contribution to the axial-vector and pseudoscalar correlators with two extra pions*, *Phys.Rev.* **D87** (2013), no. 1 014505, [arXiv:1209.2258].

[43] O. Bär, *Nucleon-pion-state contribution to nucleon two-point correlation functions*, arXiv:1503.03649.

[44] M. Lüscher, *Volume Dependence of the Energy Spectrum in Massive Quantum Field Theories. 1. Stable Particle States*, *Commun.Math.Phys.* **104** (1986) 177.

[45] M. Lüscher, *Volume Dependence of the Energy Spectrum in Massive Quantum Field Theories. 2. Scattering States*, *Commun.Math.Phys.* **105** (1986) 153.

[46] M. Lüscher, *Two particle states on a torus and their relation to the scattering matrix*, *Nucl.Phys.* **B354** (1991) 531.

[47] M. Lüscher, *Signatures of unstable particles in finite volume*, *Nucl.Phys.* **B364** (1991) 237.

[48] M. T. Hansen and S. R. Sharpe, *Multiple-channel generalization of Lellouch-Lüscher formula*, *Phys.Rev.* **D86** (2012) 016007, [arXiv:1204.0826].

[49] T. Yamazaki, *Hadronic Interactions*, arXiv:1503.08671.

[50] **ALPHA** Collaboration, J. Heitger, A. Jüttner, R. Sommer, and J. Wennekers, *Non-perturbative tests of heavy quark effective theory*, *JHEP* **0411** (2004) 048, [hep-ph/0407227].

[51] P. Fritzsch, N. Garron, and J. Heitger, *Non-perturbative tests of continuum HQET through small-volume two-flavor QCD*, to be published (2015).

[52] M. Bruno, D. Djukanovic, G. P. Engel, A. Francis, G. Herdoiza, et al., *Simulation of QCD with $N_f = 2 + 1$ flavors of non-perturbatively improved Wilson fermions*, *JHEP* **1502** (2015) 043, [arXiv:1411.3982].

[53] F. Bahr, F. Bernardoni, J. Bulava, A. Joseph, A. Ramos, et al., *Form factors for $\mathrm{B_s} \to \mathrm{K}\ell\nu$ decays in Lattice QCD*, arXiv:1411.3916.

[54] M. Della Morte, J. Heitger, H. Simma, and R. Sommer, *Non-perturbative Heavy Quark Effective Theory: An application to semi-leptonic B-decays*, arXiv:1501.03328.

[55] **ALPHA** Collaboration, U. Wolff, *Monte Carlo errors with less errors*, *Comput.Phys.Commun.* **156** (2004) 143, [hep-lat/0306017].

[56] **ALPHA** Collaboration, S. Schaefer, R. Sommer, and F. Virotta, *Critical slowing down and error analysis in lattice QCD simulations*, *Nucl.Phys.* **B845** (2011) 93, [arXiv:1009.5228].

[57] **ALPHA** Collaboration, H. Simma, R. Sommer, and F. Virotta, *General error computation in lattice gauge theory*, Internal notes of the ALPHA collaboration (2014).

[58] **ALPHA** Collaboration, S. Lottini and R. Sommer, *Data analysis in lattice field theory*, lectures with exercises given at *Lattice practices,* DESY, Zeuthen (2014). https://indico.desy.de/conferenceDisplay.py?confId=9420.

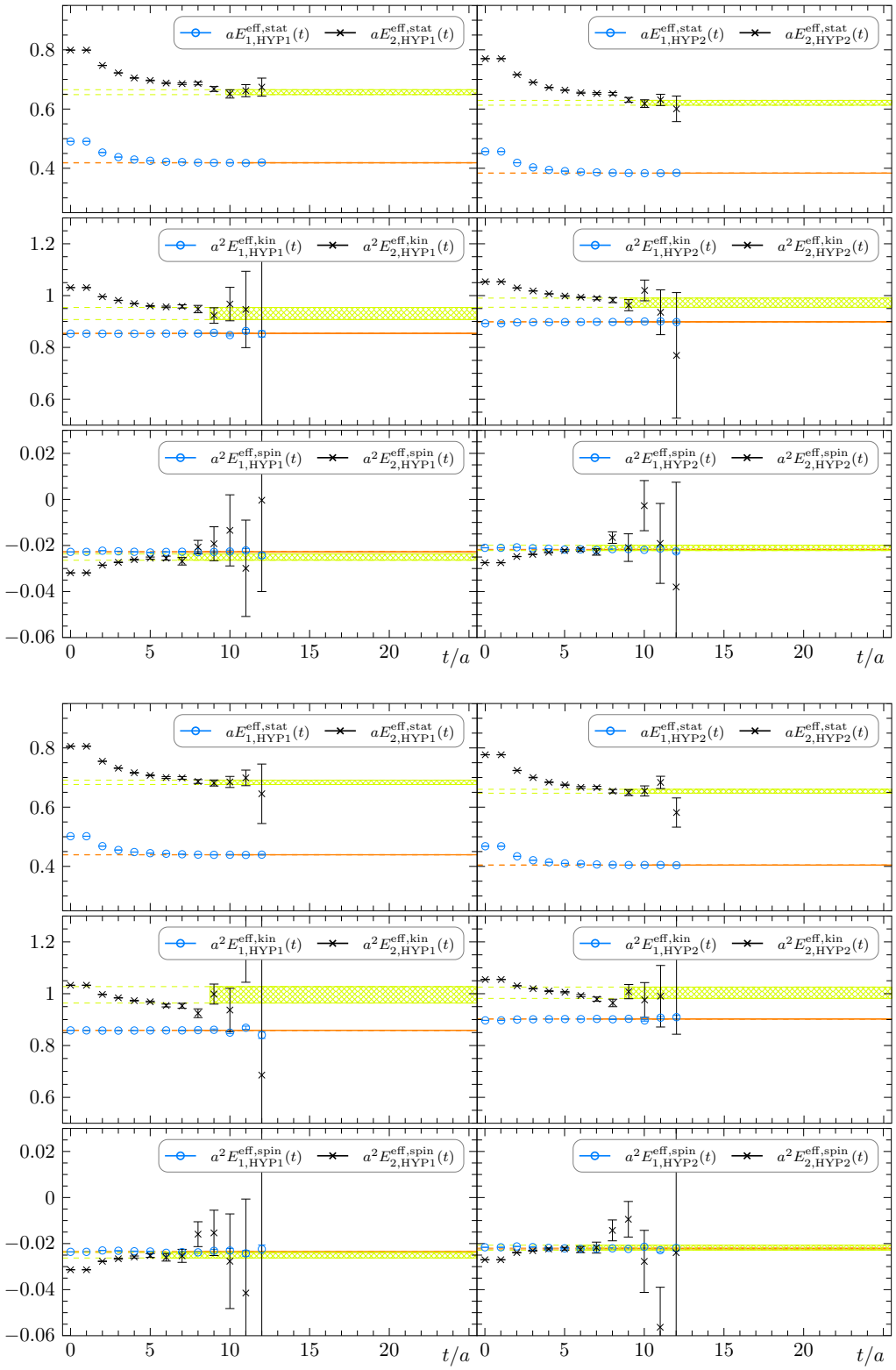

Figure 7: Effective energies $E^{\mathrm{eff,x}}_{n,\delta}$ following our GEVP analysis in the heavy-light (*top*) and heavy-strange (*bottom*) sector on ensemble A4.

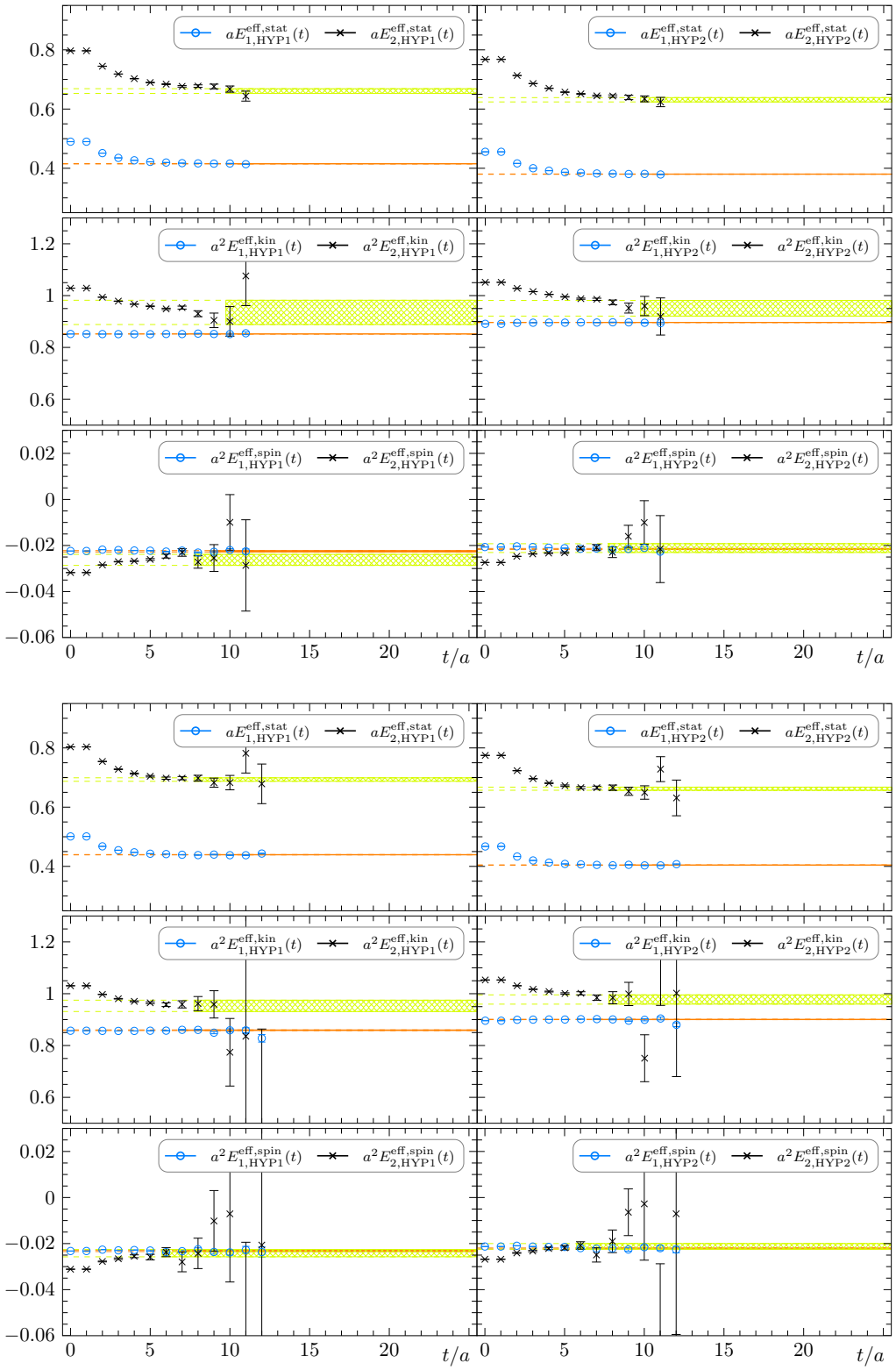

Figure 8: Effective energies $E^{\mathrm{eff,x}}_{n,\delta}$ following our GEVP analysis in the heavy-light (*top*) and heavy-strange (*bottom*) sector on ensemble A5c.

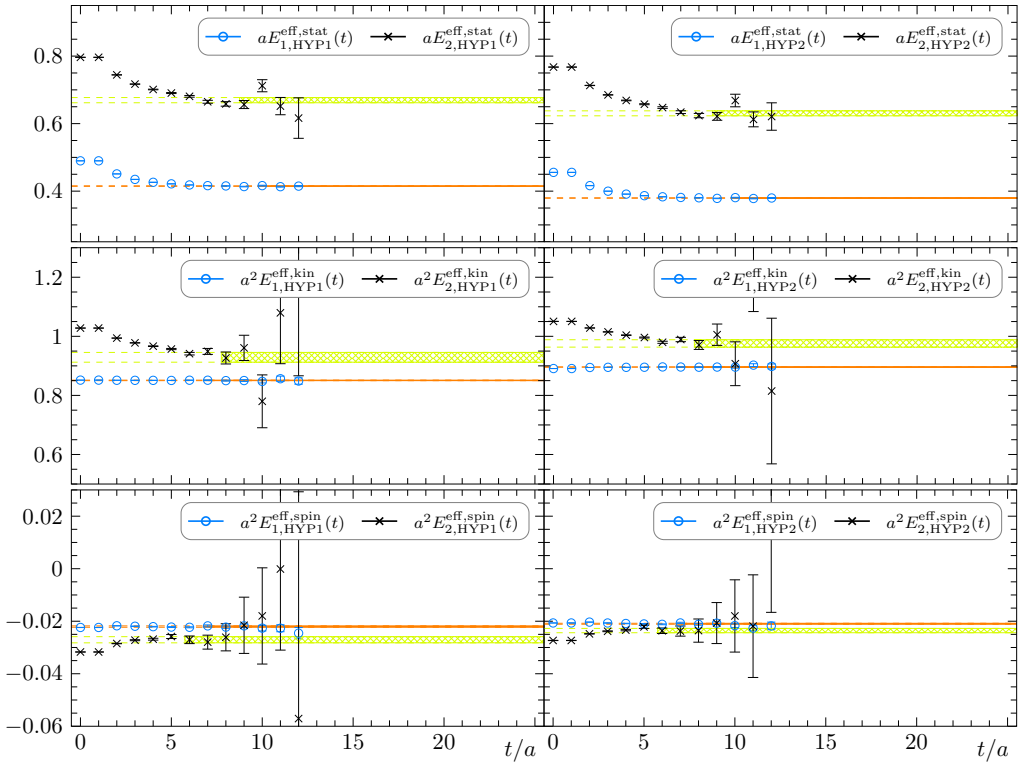

Figure 9: Effective energies $E^{\mathrm{eff,x}}_{n,\delta}$ following our GEVP analysis in the heavy-strange sector on ensemble A5d.

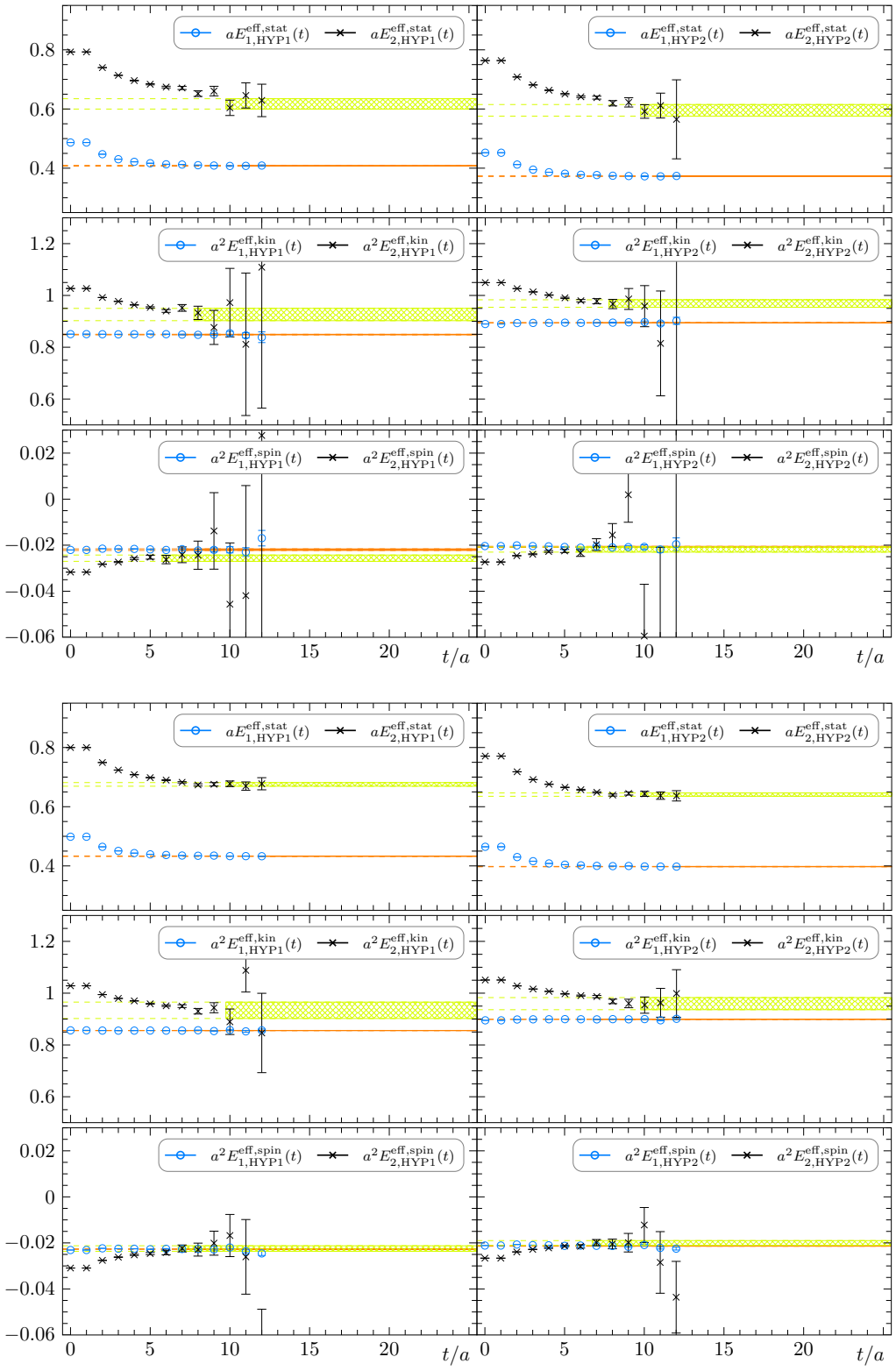

Figure 10: Effective energies $E^{\mathrm{eff,x}}_{n,\delta}$ following our GEVP analysis in the heavy-light (*top*) and heavy-strange (*bottom*) sector on ensemble B6.

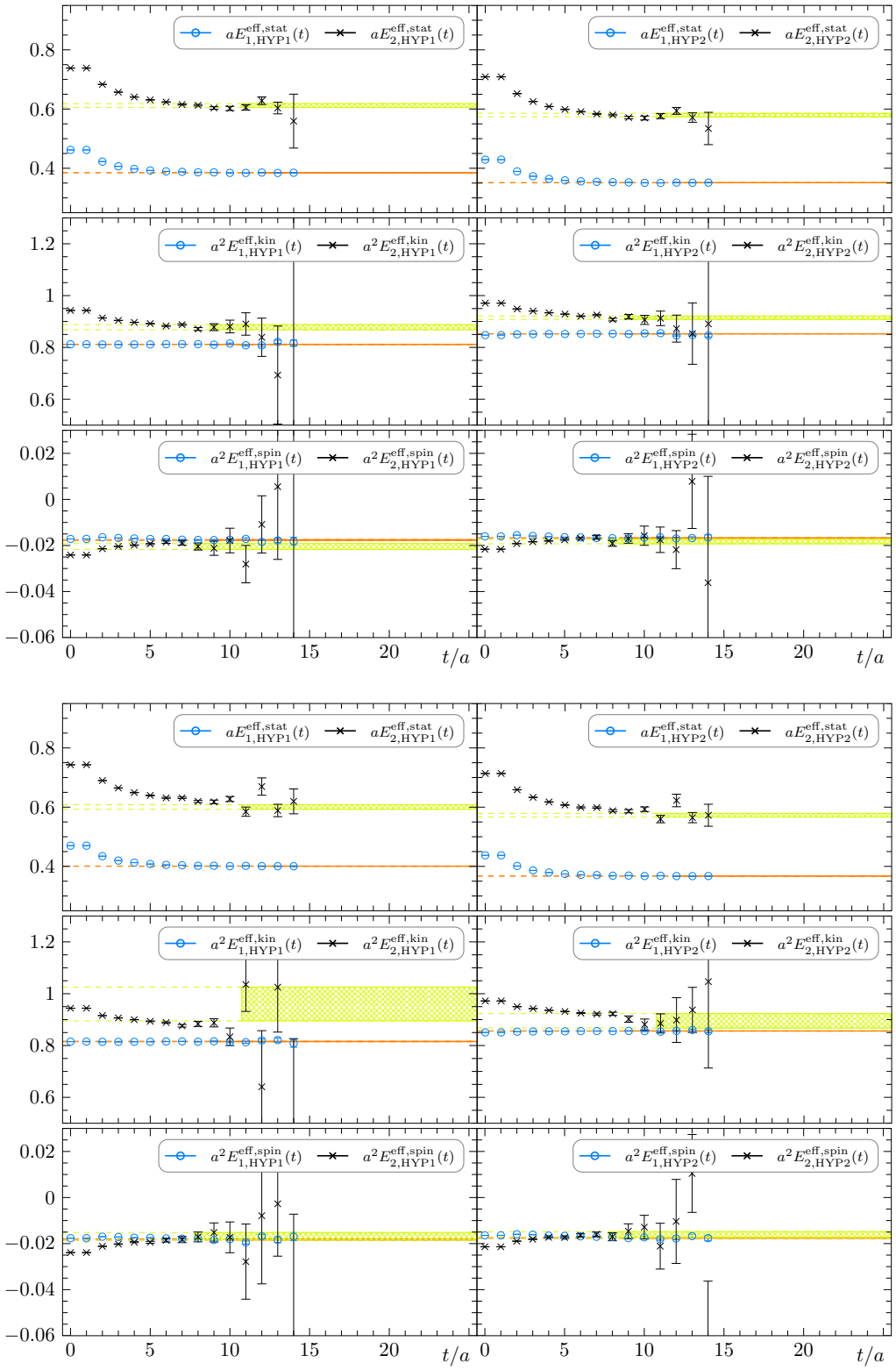

Figure 11: Effective energies $E^{\mathrm{eff,x}}_{n,\delta}$ following our GEVP analysis in the heavy-light (*top*) and heavy-strange (*bottom*) sector on ensemble E5g.

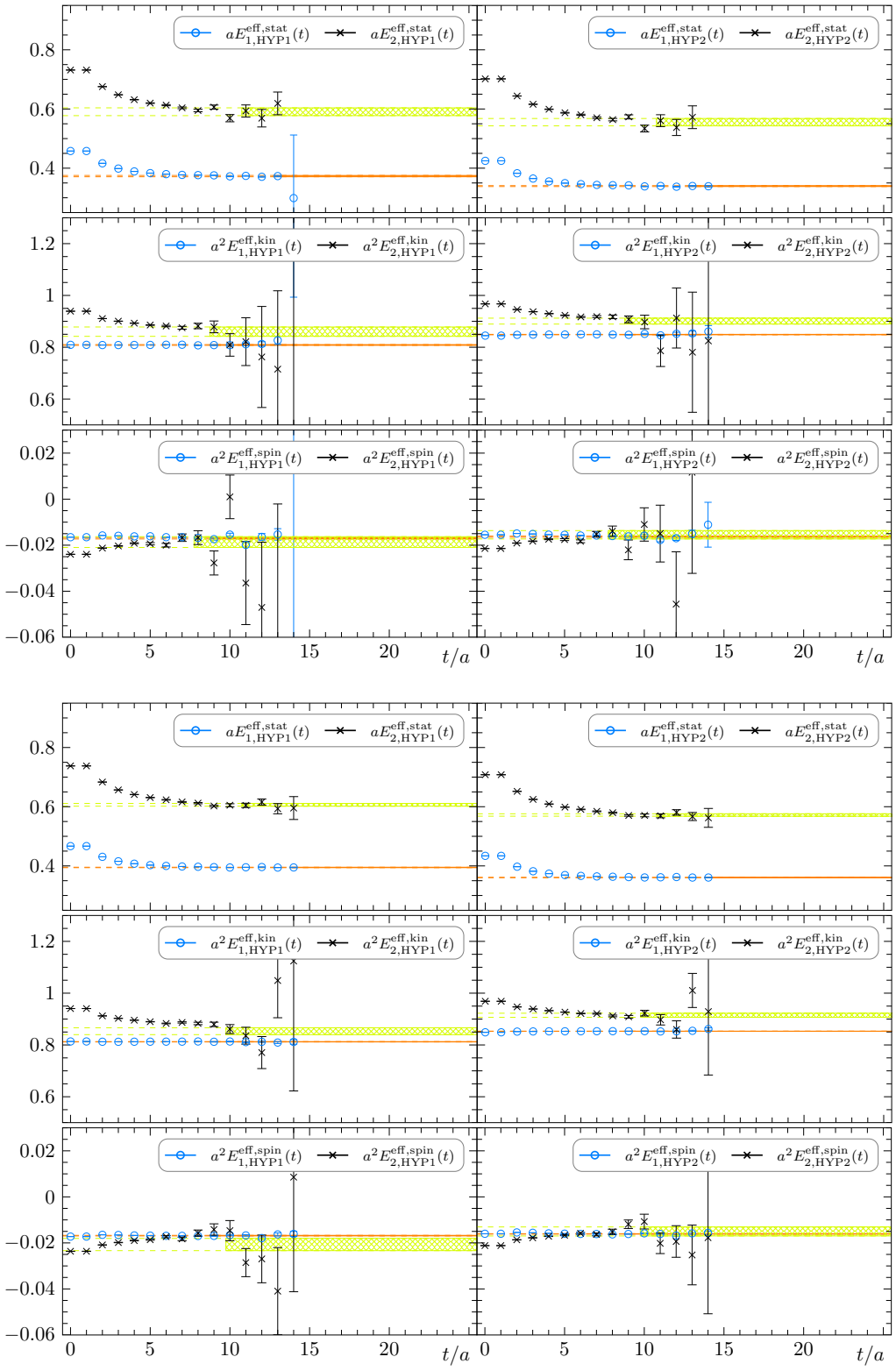

Figure 12: Effective energies $E^{\mathrm{eff,x}}_{n,\delta}$ following our GEVP analysis in the heavy-light (*top*) and heavy-strange (*bottom*) sector on ensemble F6.

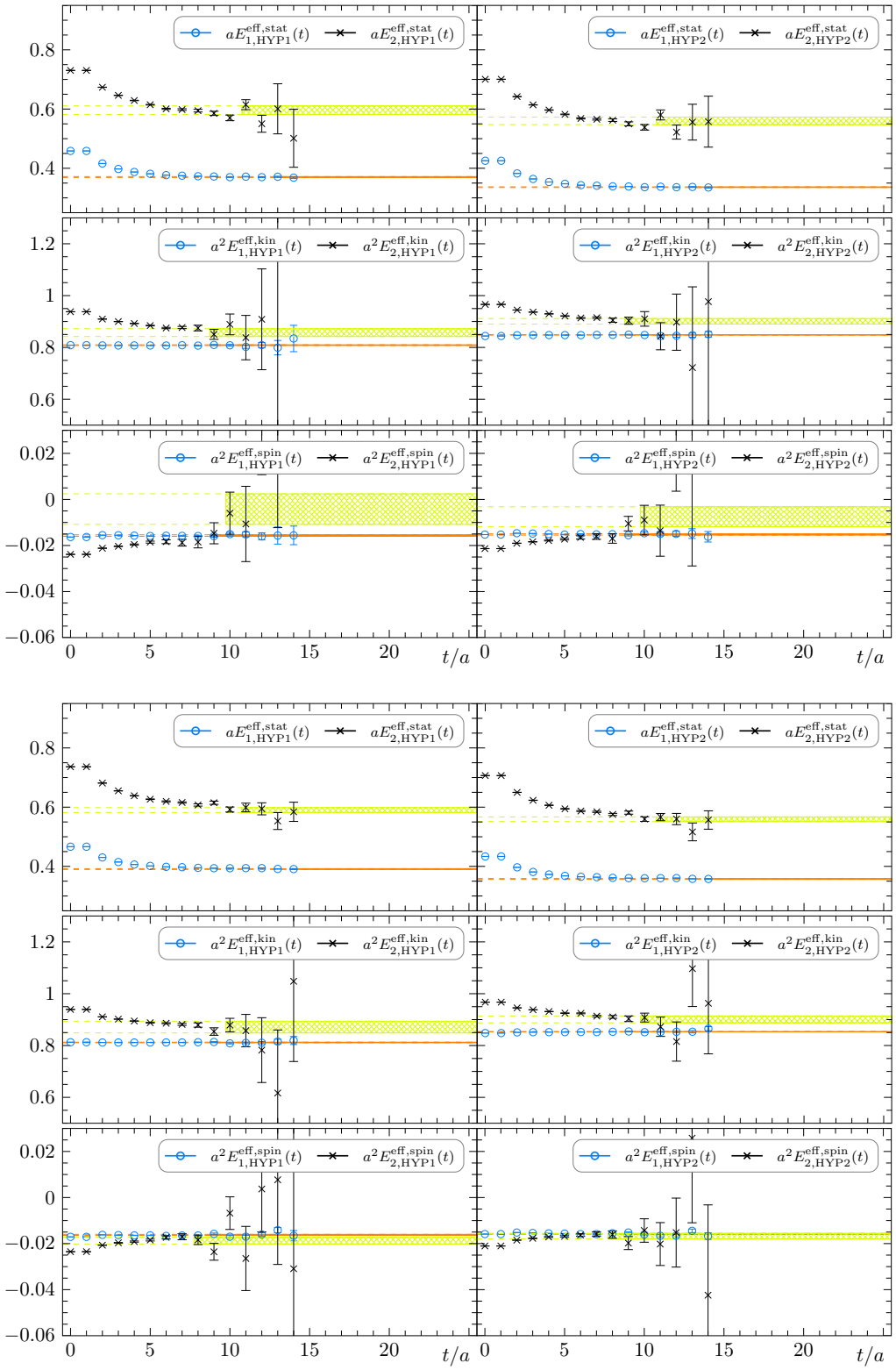

Figure 13: Effective energies $E^{\mathrm{eff,x}}_{n,\delta}$ following GEVP analysis in the heavy-light (*top*) and heavy-strange (*bottom*) sector on ensemble F7.

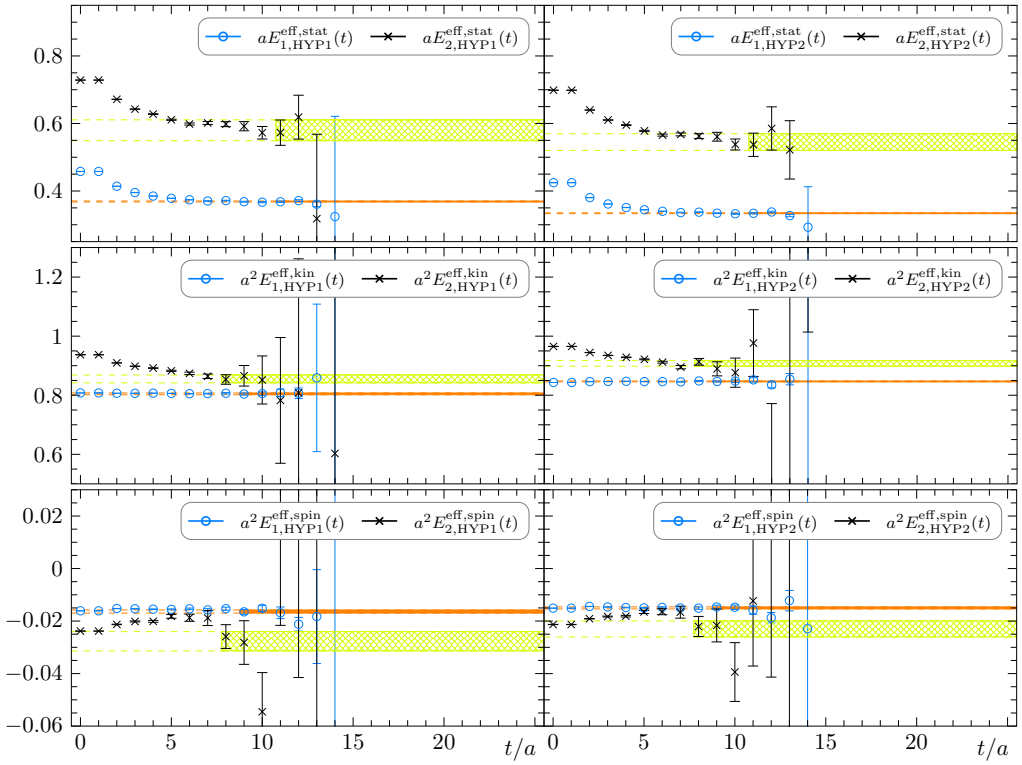

Figure 14: Effective energies $E^{\mathrm{eff,x}}_{n,\delta}$ following our GEVP analysis in the heavy-light sector on ensemble G8.

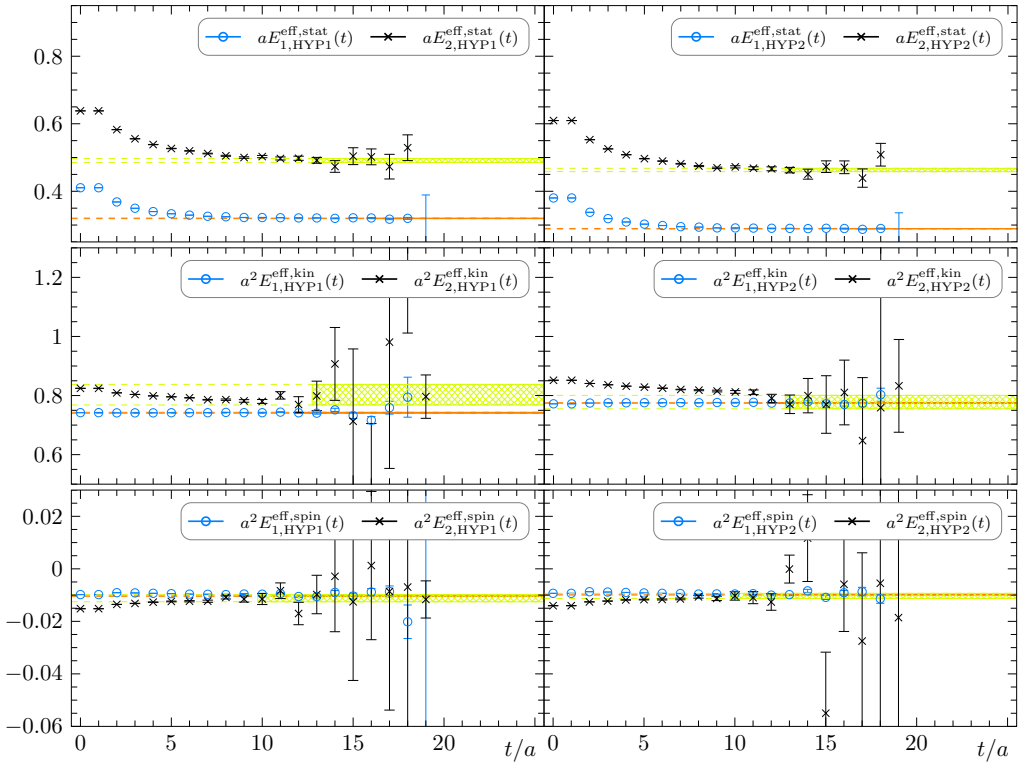

Figure 15: Effective energies $E^{\mathrm{eff,x}}_{n,\delta}$ following our GEVP analysis in the heavy-light sector on ensemble N5.

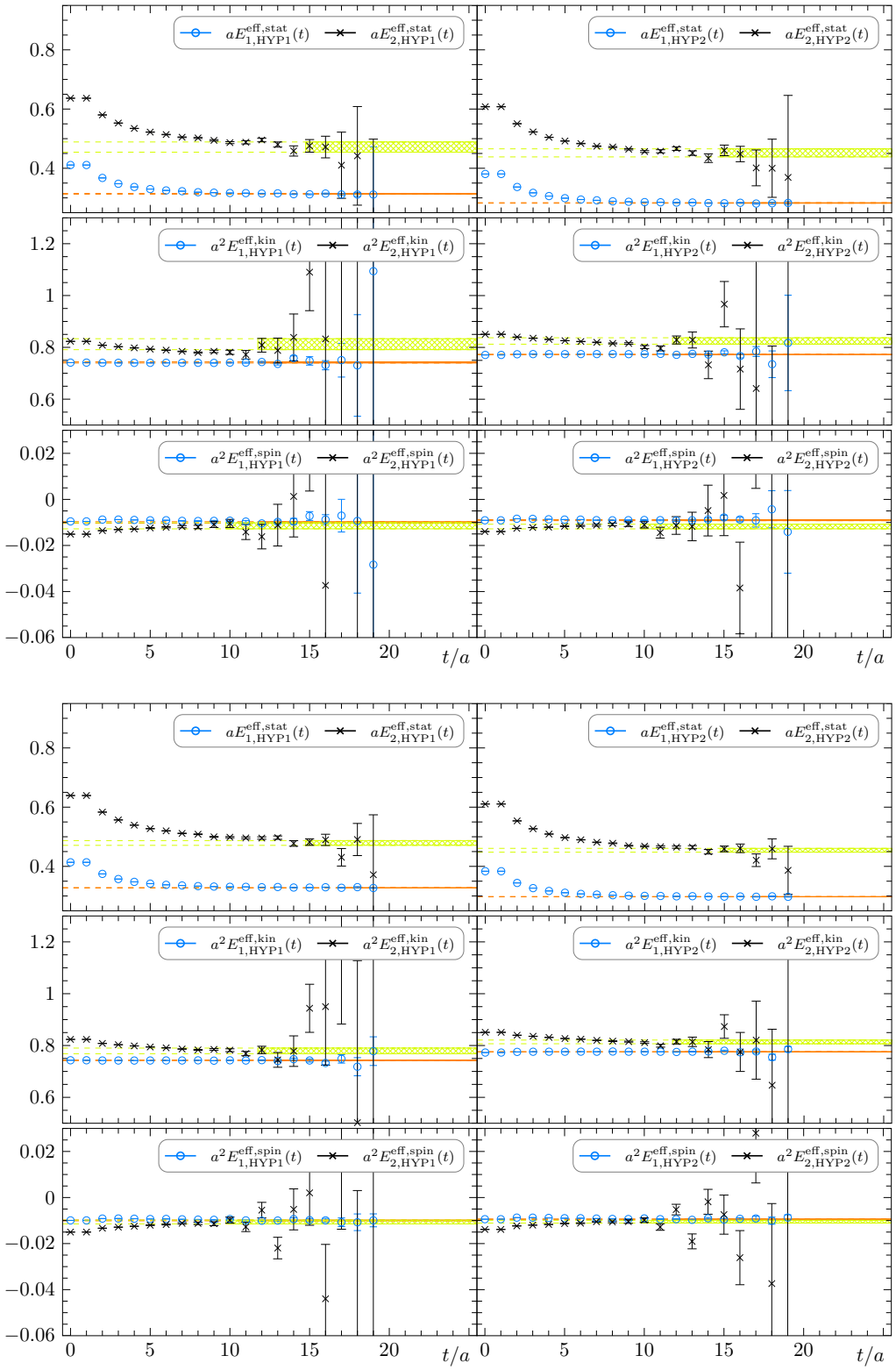

Figure 16: Effective energies $E^{\mathrm{eff,x}}_{n,\delta}$ following our GEVP analysis in the heavy-light (*top*) and heavy-strange (*bottom*) sector on ensemble N6.

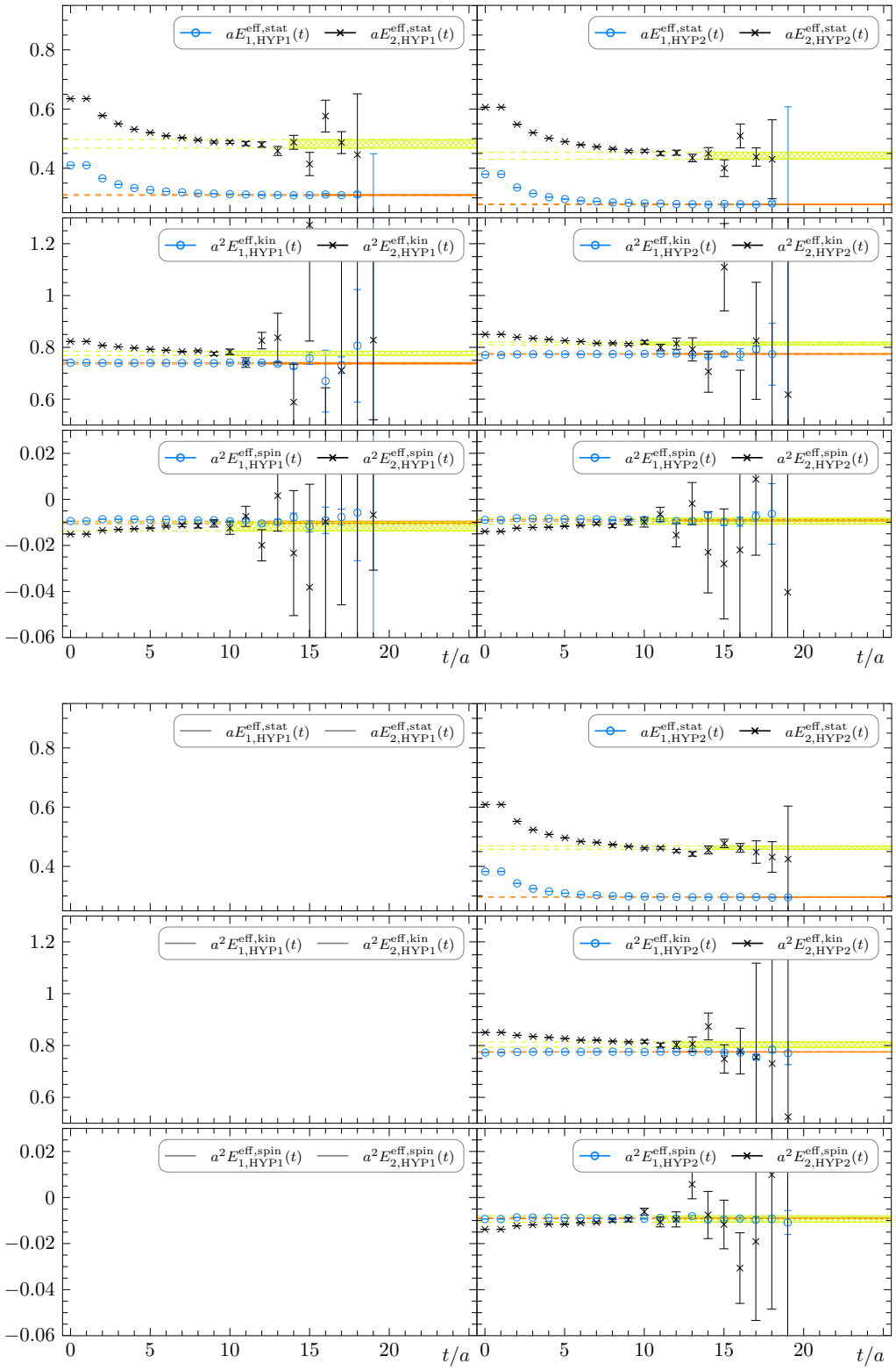

Figure 17: Effective energies $E^{\mathrm{eff,x}}_{n,\delta}$ following our GEVP analysis for heavy-light (*top*) and heavy-strange (*bottom*) sector on ensemble O7c.